Fault Tolerant Control and Reliability Assessment of Modular PMSM Drive Systems

by

Ing. O. Nobel

in partial fulfilment of the requirements for the degree of

Master of Science
in Electrical Engineering

at the Delft University of Technology,
to be defended publicly on Tuesday September 11, 2018 at 10:00

Thesis committee:

Prof. dr. P. Bauer	(Supervisor)
Dr. J. Dong	(Daily supervisor)
Dr. ir. J.L. Rueda Torres	

An electronic version of this thesis is available at http://repository.tudelft.nl/.
Cover page image: [1]

TU Delft Delft University of Technology

Abstract

This report proposes an approach to implement improved Fault Tolerant (FT) control in a modular Open Winding (OW) Permanent Magnet Synchronous Machine (PMSM) drive system. The report also proposes a reliability assessment on FT converter topologies and the effect of layering redundancy. An existing lab setup is used as a case study to create a new control system. The redundant case functions with multiple sets of phases, a fault will disable the faulted set leaving the sound phases operational.

The new system aims to utilise all remaining sound phases (5 out of 6) in case of an OCF. Operating the drive system in this post-fault condition will leave the system unbalanced, leading to Common Mode (CM) voltage and current. The new system therefore has to operate with the remaining sound phases, whilst reducing the CM disturbance. It is expected that this can be achieved by modifying the control system. Expanding the control system from dq to dq0 allowed control of the zero-sequence current, the CMC.

Applying the CMR control allows reduction of CMC in pre- and post-fault condition at nominal load. For post-fault this did result in a current overload of 344.21% in one of the stator phases relative to the pre-fault current. This overload should be taken into account when designing a machine for a specific applications by reducing the post-fault load or over-sizing the machine. The CMR control system proposes an approach to control the machine and reduce the CMC during post-OCF condition.

The reliability assessment compared traditional VSI to OW to the extra switching leg converter. Each assessed for one, two and three sets of three phases, also for split and common DC bus. The extra switching leg and OW topology showed the highest reliability across all phase set configurations. The application of a common DC bus has greatly reduced reliability compared to a split DC bus. The reliability gain of the extra switching leg and OW converter is relatively small compared to the traditional VSI, it is concluded that the traditional VSI is a cost effective converter for achieving FT, if applied redundant.

Acknowledgements

First, I would like to thank dr. Jianning Dong for the support he has given me performing this thesis. His openness and and critical attitude helped me perform to the best of my abilities. He was always willing to respond to any questions and consistently allowed this report to be my own work, whilst steering me in the right direction when necessary. I would like to acknowledge prof. dr. P. Bauer and dr. ir. J.L. Rueda Torres for attending the thesis defence and reading the thesis report.

Many thanks to my partner for sharing this thesis period with me. For reading, providing feedback and discussing approaches for the project and the report. I also very much appreciate the times I did not have to do the dishes or get groceries, leaving me with more time to work on the thesis. I would like to thank my parents for their support both economic and emotional. Especially given that I have already obtained a degree. I would also like to thank my sister for her unconditional support.

List of Acronyms

- CCW - Counterclockwise
- CM - Common Mode
- CMC - Common Mode Current
- CMV Common Mode Voltage
- CW - Clockwise
- DC - Direct Current
- DE - Differential Equations
- DTC - Direct Torque Control
- F - Faulted (state)
- FOC - Field Oriented Control
- FT - Fault Tolerant
- H - Healthy (state)
- HF - High Frequency
- Hw - Hardware
- IM - Induction Machine
- ISC - Indirect Stator Control
- LC - Linear Combination
- MC - Microcontroller
- MPC - Model Predictive Control
- OCF - Open Circuit Fault
- OW - Open Winding
- PMSM - Permanent Magnet Synchronous Machine
- PWM - Pulse Width Modulation
- RM - Reluctance Machine
- SCF - Short Circuit Fault
- SM - Synchronous Machine
- SRM - Switched Reluctance Machine
- SVPWM - Space Vector Pulse Width Modulation
- Sw - Software
- VSI - Voltage Source Inverter
- ZVPWM - Zero Voltage Pulse Width Modulation

Contents

List of Figures

List of Tables

1 Introduction

1.1. Background

Engineers are continuously aim to increase the performance of the system. The performance can be expressed in values like: cost, size, weight, efficiency, reliability etc. another example of a performance value is availability, which relates to the time that the system is able to perform its function. An application that required a high availability can be found in aerospace engineering. This, in combination with the electrification of aircraft in More Electric Aircraft (MEA), leads to increased interest in drive systems with high availability. Fault Tolerant (FT) systems is one of the research topics that aims to improve availability. Allowing a system to continue operation when subjected to a fault is intuitive for this. Currently there is consensus regarding an optimal solution for FT drive systems.

1.2. Motivation

A common approach to obtain high system availability is by implement redundancy. The drawback with this approach is an (unnecessary) increase in cost, weight or complexity. This offers an opportunity for improvement. It is therefore aimed to present an approach for a drive system with high availability, without solely relying on redundancy.

Publications on FT control often approach the problem for specific converter topologies. However, this leaves the comparison between the possible topologies. In order to reach a high available drive system control, converter and machine have to be optimised. Providing a comparison on any of thesis topics would contribute to reaching a consensus.

1.3. Objectives

The background and motivation are used to formulate the objectives of this thesis. This thesis aims to find a FT control system for the existing drive system. This proposal should be an improvement over achieving FT only by redundancy. The second objective is to contribute to a comparison of FT drive system approaches. Starting with a reliability assessment on the converter topologies can also directly lead to recommendations to improve the existing drive system [1]. The objectives are summarised as follows:

1. Provide an overview on FT drive systems.
2. Improve the existing drive system
   - Determine the performance of the existing drive system.
   - Formulate a solution for a new control system that improves the existing drive system with regard to FT and the CMC.
   - Verify the new control system by comparing the simulated performance to the original control system.
3. Assess the reliability of FT converter topologies.

1.4. Methodology

Each of the defined objectives are associated with a methodology to structure the approach:

1. An overview on FT drive systems can be presented by studying publications on the relating topics. This gives direction to the rest of the project. Topics that are considered are divided into: Control, converter and machine with regard to FT.
2. A case study is performed to improve the existing drive system. The existence of this drive system allows a specially designed a control system. Simulating the drive system in the original and the new case allow a the verification of the results.

Figure 1.1: Methodology - Case study - Drive system improvement

3. The reliability assessment aims to provide a generalised comparison on FT converter topologies. Examples of FT converter topologies have to be defined, these will be obtained from the literature study. FT converters have the inherited capability to operate when subjected to one (or sometimes multiple) faults. Markov chain models offer a tool to incorporate the operation modes of the converter topologies.

1.5. Contribution

This thesis aims to contribute to improving the existing drive system. An improvement will contribute to a working prototype of a FT drive system, as could be applied in aerospace engineering. This will allow further electrification of aircraft, leading to an increase in efficiency and reducing fuel consumption [2]. The reliability assessment will lead to an attempt of reaching a consensus on FT drive systems. Markov chain models could also be applied in a similar approach to analyse systems with multiple operating states.

2

Overview of Fault-tolerant electrical drives

This chapter covers a literature study aiming to explore the state of academic knowledge regarding FT drive systems. Increasing understanding of the topic and providing a focus when formulating a solution. The knowledge obtained through the literature will be used to analyse the available lab setup. This knowledge will also contribute to the formulation of an improved FT control system. Several definitions on subsystems and topologies will be defined in this chapter which will be applied in later chapters.

2.1. Fault tolerance

The implementation of FT has to be studied in each subsystem in order to formulate an approach for FT in the system as a whole. Several studies were performed in order to formulate a definition for FT [3][4]. A set of specifications were proposed that define a FT drive system. An alternative approach to the defining FT is proposed by J.J. Wolmarans *et al.,* [5] stating that: ***"No single electrical fault may cause the system as a whole to stop functioning"***. Confining to electrical faults, aspects outside the electrical domain regarding fault origin is not in the scope of this thesis.

Two aspects can be formulated for FT drive systems. The first is by designing the system in such a way that it facilitates FT. Achieved by designing a system that separates the critical functions of the system. Some form of redundancy is always incorporated as there is always a non-zero chance of a component failure. Faults should be isolated to leave room for FT control. A FT facilitated system is able to be controlled in such a way that the system as a whole becomes FT. There are several approaches that facilitates FT, each resulting in different control strategies. Hardware design choices of the machine and power converter have to be made before designing a FT controller, as these subsystems dictate the system properties.

2.2. Drive system

A drive system is a system that converts electric to mechanical energy and *vice versa*. One approach to define a drive system is by performing a decomposition into subsystems, as illustrated in figure 2.1. At the core of this system is the electric machine. The conversion between electric and mechanical energy takes place here. There are several types of machines, each having different attributes. The second subsystem is the power converter, included in applications that require some form of control. The function of a power converter is the conversion of a (semi) fixed electric supply to the desired AC waveform for the machine. Control signals are generated by first measuring the feedback signals from the machine.

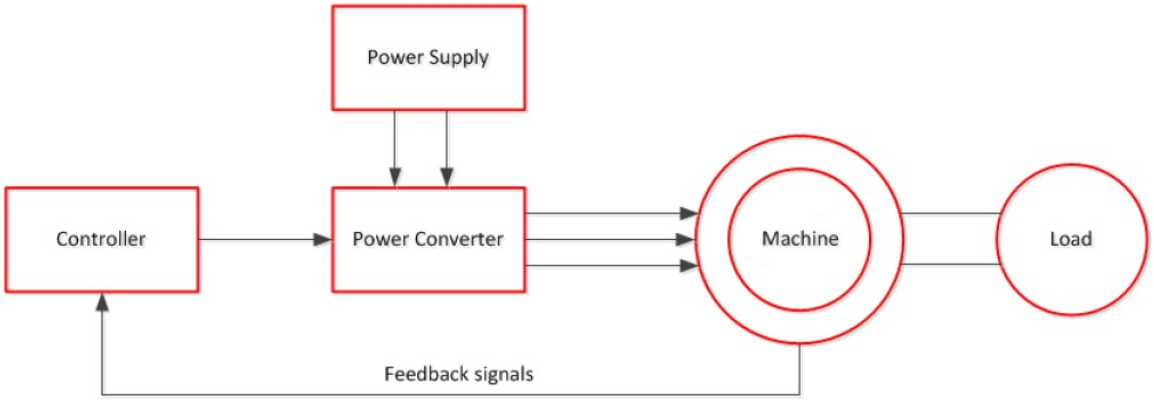

Figure 2.1: Subsystem decomposition drive system – Adapted version [1]

2.3. Electric machine comparison

The machine is one of the subsystems proposed in paragraph 2.2. A general aspect of an electric machine is its type. Several main types of electric machines are discussed: The Asynchronous or Induction Machine (IM), The Reluctance Machine (RM) and the Permanent Magnet (PM) machine.

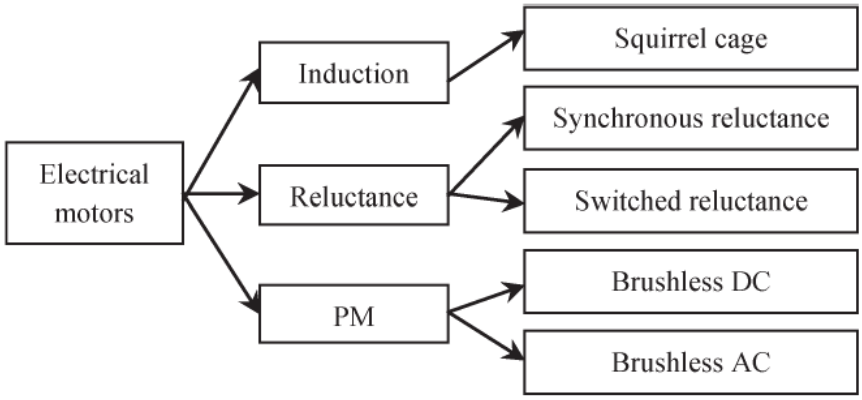

Figure 2.2: Machine types for FT drive systems [2]

Several studies were found discussing FT in electric machines [4][6][7]. The main attribute for systems operating in an aircraft is that it should have a high power to mass ratio [4]. FT and reliability are also requirements for a system to function in this application field. Table 2.1 presents a performance comparison of three machine types. The performance of the IM seems to be sub-par to the other machine types. The intrinsic FT for the RM is one of the reasons this type is often applied for FT applications [2]. The high efficiency and power density of the PM machine presents this type as a possible candidate for improvement over the RM. Each machine type as categorised in figure 2.2 will be discussed for FT in the following paragraphs.

Table 2.1: Machine option performance comparison [2]

Performance	**IM**	**RM**	**PM**
FT (intrinsic)	Low	High	Low
Power density	Moderate	Moderate	High
Efficiency	Moderate	High	High
Cost	low	low	high

2.3.1. IM - squirrel cage

The IM is a common machine type often applied in motor applications. The power density of the IM is lower compared to the PMSM [2]. The low inherited FT makes this machine not suitable for FT aerospace application as it offers no potential improvement over the utilisation of a SRM. It is also impossible to effectively split the stator phases due to the permanent magnetic coupling [2], making fault isolation difficult.

2.3.2. Synchronous RM

Reluctance machines do not utilise windings or permanent magnets in the rotor to operate. The RM is also able to withstand large mechanical and thermal stress. No back EMF from the PM is induced at synchronous speed allowing for a high steady state efficiency [2]. The distributed windings of this machine type do form a strong coupling between the stator phases, making phase separation difficult. Phase separation is an important aspect for FT systems to isolate faults.

2.3.3. Switched RM

The Switched Reluctance Machine (SRM) was a commonly applied machine type for aerospace application, due to its inherited FT [2]. This is the case even with reduced power density compared to other machine types [3][4][8]. The stator and rotor each have salient poles making the phase windings independent. The desire to reduce system weight is a point of improvement when choosing a machine type for FT applications. A possible candidate therefore has to be able to incorporate FT whilst having a higher power density compared to the SRM.

2.3.4. PMAC

Brushless DC and AC can be grouped under the category of PMAC machines [2]. PM machines can be designed in multiple ways. Design decisions cover: changing the magnet configuration in the rotor and the winding arrangement in the stator. Surface mounted magnets and concentrated windings are often applied for FT machines [2]. A PM machine can be designed with a smaller size whilst being equally fault-tolerant compared to a SRM [7]. The PM in the rotor results in permanent existence of the rotor field. A current will be flowing in case of a SC in the stator winding, this current is generated by the induced back-EMF. The PMSM is not inherently FT, this has to be incorporated separately. This machine type can be considered the main candidate for this study for improved FT drive systems.

2.3.5. Modular multiphase design

An extensive review study by E. Levi [9] regarding the multiphase machine application discusses multiphase machine design in combination with FT. Modularity can be achieved in individual phases, in phase sets or in both. A modular design allows the separation of stator phases, improving fault isolation. Another advantage of a multiphase machine is a higher reliability and increased torque density at reduced torque ripple versus regular machines [11]. Applying a modular multiphase machine is proposed in studies as a strategy to achieve a FT drive system [9][11]. Having more than three phases leaves the possibility to revert to a post-fault control state that relies on radial symmetry. A modular design of a multiphase machine allows the uniformisation of the stator phases. Another advantage of applying modular design is that the electric power can be distributed over all phases, effectively reducing the nominal per phase power.

2.3.6. Winding configuration

One consideration that can be made when designing the stator windings, is the magnitude of the stator inductance. The stator inductance should be large enough to limit the fault current to the nominal current [5][11]. This will negate the possibility of isolation damage in the windings due to increased temperatures, which negates the possibility of a fire cause by a short circuit. The mutual inductance should be small in order to isolate the sound phases from the faulted phase. Two categories for winding configurations are concentrated and distributed windings. Concentrated windings have an advantage over distributed windings for facilitating FT. Reason for this is the physical separation of the stator phases, negating the possibility of a phase to phase isolation fault [5][11].

2.4. Overview of FT Power converters

Complex energy systems rely on power converters to control the flow of electric power. One important design decision when designing a power converter is how to implement a neutral connection. The following strategies can be derived: One neutral connection, multiple neutral connections and no neutral connections. Implementing one neutral connection for a FT systems seems counter intuitive as it connects all the stator phases to one common link, which could fail. Another possibility is to extended to a design with multiple neutral connections per set of (symmetrical) phases into a multiphase configuration [9]. The most intuitive solution for FT would be to incorporate no neutral connection, this can be achieved by the implementation of H-bridge inverter legs. Utilising H-bridge converters without a neutral connection allows individual phase control. Allowing more degrees of freedom, but adding the challenge of managing (Common Mode) zero-sequence currents [10]. Studies regarding FT power converters are often restricted to specific topologies. The choice of topology severely impacts the way FT can be implemented. The following paragraphs will therefore discuss several FT converter topologies.

2.4.1. Dual three phase with split DC bus

The first topology is that of a dual three phase converter, which is designed to operate for a six phase machine achieving FT by applying redundancy. This system functions as two separate systems, a single fault in one converter will leave the other intact. Figure 2.3 visualises the redundant dual three phase converter topology [13]. The idea behind this strategy is to utilise the mature technology of traditional power converters resulting in relatively simple implementation. The appliance of redundancy guarantees that this sound phase set remains functional in case of a fault. The disadvantage of this strategy is that the post-fault nominal power is reduced to 50%. Another disadvantage is that two converters double the cost and the failure rate of a single converter.

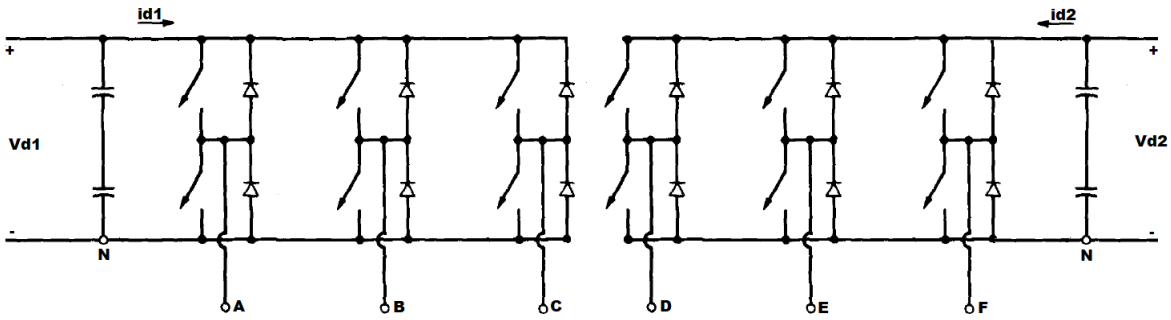

Figure 2.3: Schematic overview of a dual three phase converter - split DC bus - Adapted version [13]

2.4.2. Dual three phase with common DC bus

An alternative approach to the dual three phase converter was proposed by W. Wang *et al.,* [14]. Regarding FT control in a dual three phase configuration subjected to IGBT Open Circuit Fault (OCF). The six stator phases are connected to a common DC bus, as visualised in figure 2.4. This topology is separated from others by the two star point connections for each set of three phases, negating the problems with CM disturbance. Two post (OCF) fault control strategies are proposed: Loss-mode (minimising copper loss) and Torque-mode (maximising torque). Which strategy depends on the requirements in post-fault condition.

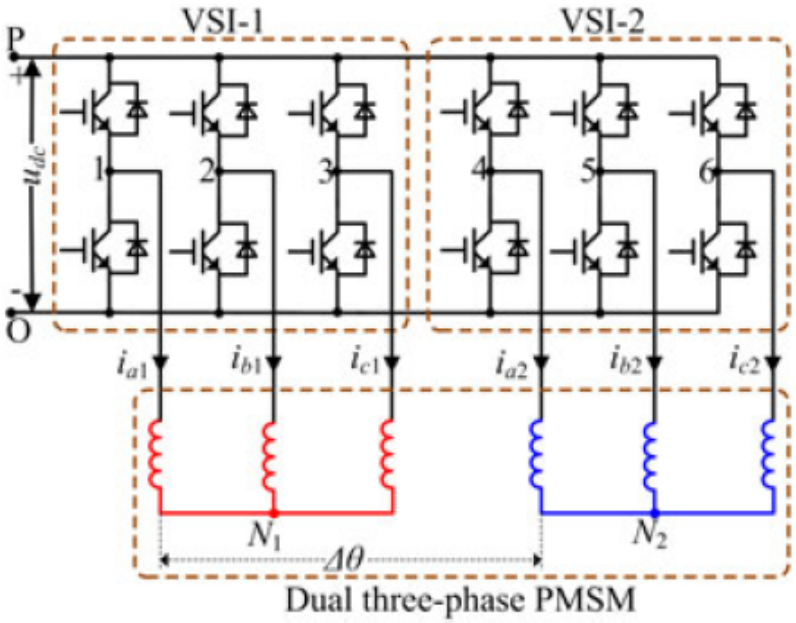

Figure 2.4: Schematic overview of a dual three phase converter - Common DC bus - Adapted version [14]

Controlling the machine in Loss-mode is achieved by deactivating the faulted phase and continue operation by the remaining five sound phases. This is possible due to the star point connection negating the circulation of CM currents (CMC). Loss-mode is achieved by reducing the reference signal preceding the Park transformation [14]. Torque mode is achieved by increasing the transformation constant up to the physical limitation of the phase current. This increases the copper losses and the maximum available torque.

2.4.3. Extra switching leg converter

Another topology for FT converter was proposed by O. Wallmark *et al.,* [15]. This proposal considers the addition of an extra switching leg connected to the star point of the machine, as visualised in figure 2.5. Aimed to accommodate FT should a phase become isolated due to a fault. The added switching leg will switch the neutral point to accommodate FT. An expansion on the traditional converter to incorporate FT. This study is constrained by assuming phase isolation for fault mode. This assumption does not cover SCF.

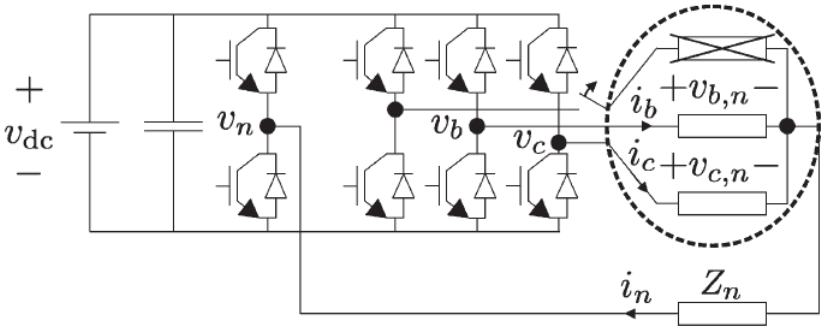

Figure 2.5: Schematic overview of an Extra switching leg converter - Three phase - Adapted version [15]

The same study argues that applying this method will reduce the post-fault output power. Therefore an expanded topology is suggested in figure 2.6 negating this con. This figure shows the expansion of the converter to a dual three phase converter with common DC bus whilst retaining the added switching

leg. Expanding the drive system to six phases with a common DC bus does increase the complexity of the system. The added switching leg can be realised once and applied to either set of phases reducing the requirement for redundancy.

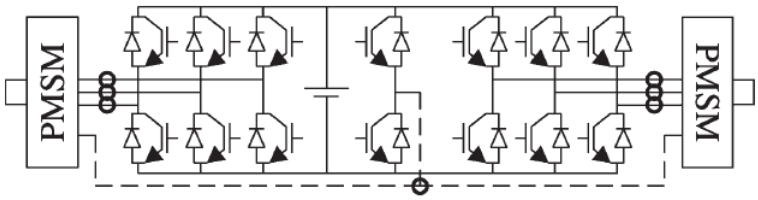

Figure 2.6: Schematic overview of an Extra switching leg converter - Six phase - Common DC bus - Adapted version [15]

2.4.4. Open Winding

Standard inverter switching legs operate with two semiconductor modules per phase. Utilising H-bridge converter doubles the semiconductor modules to four per phase. Both ends of the stator winding are connected to a converter leg instead of a neutral connection. This increases the complexity of the system as both ends have to be actively controlled. Utilising H-bridge converters also has the effect that the total failure rate in one of the semiconductor device doubles. Incorporating H-bridge modules increases the fault probability of the converter but simultaneously isolates the phase modules facilitating FT, increasing chance but reducing impact. This converter topology is called: Open Winding (OW).

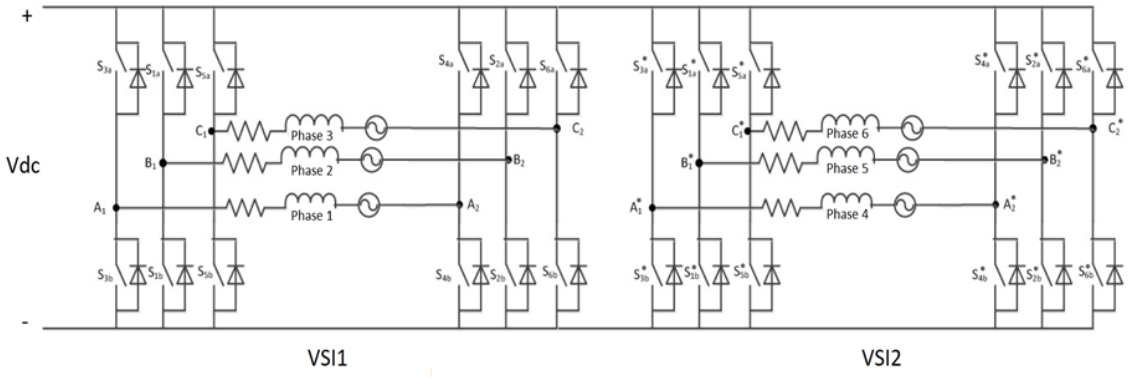

Figure 2.7: OW common DC converter topology - Six phase - Adapted version [1]

Two OW topologies are found in literature, OW with and without common DC bus (figure 2.7 and 2.8). The result of applying a common DC bus is that only one rectifier and isolation transformer will have to be applied [16], reducing the overall system weight. Applying one rectifier inherits a lower failure rate versus two rectifiers, as this chance increases linearly. A fault in a one rectifier does mean that the system will stop functioning, which is not FT. The second aspect is the manifestation of CMC. The CMC generated will, in case of a common DC buss, flow between the left and right side converter [17]. Applying a common DC bus results is the necessity to reduce the CM disturbance. The negative effects of CM disturbance is not solved when applying a split DC bus topology. The CM Voltage (CMV) will no longer cause circulating CMC but will still result in shaft voltage and bearing current that shortens the lifespan of the machine [18].

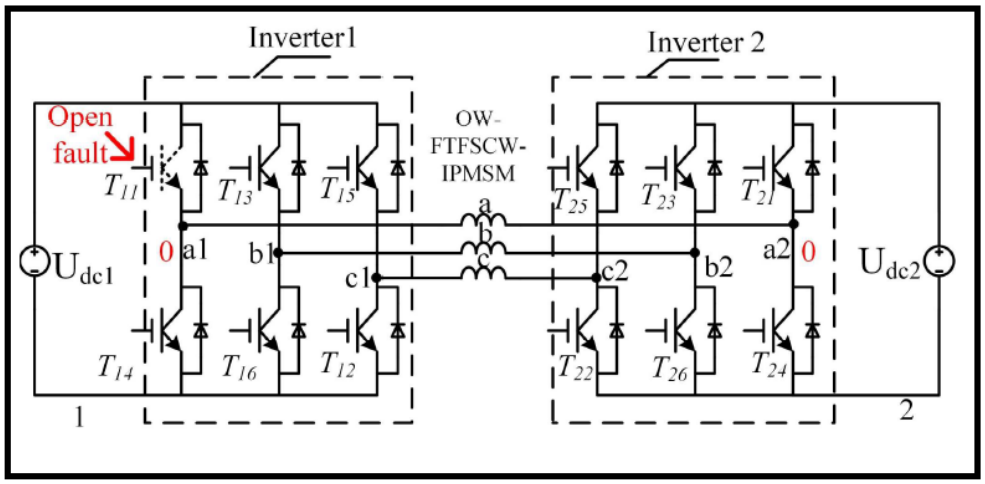

Figure 2.8: OW split DC converter topology - Three phase - Adapted version [19]

2.5. FT drive control

Comparing the machine types for aerospace applications leave the PMSM as the primary candidate for the machine type. The PMSM does not inherently facilitate FT, this has to be investigated. Several design aspects can be taken into account when designing a FT PMSM. A study by B.C. Mecrow *et al.,* [3] formulates key properties of such a design for the stator phases, these are summarised below:

- Electric isolation.
- Implicit limitation of fault currents.
- Effective thermal isolation.
- Physical isolation.
- Multiple phases.

Electric isolation is achieved by physically separating the stator phases. One approach to do so is by incorporating modular design (paragraph 2.3.5). Each module can then be separated to a different segment of the machine. Concentrated windings can be utilised opposed to distributed windings, as it physically separates the stator windings in the machine. Negating the possibility of a winding to winding failure. A fault current can be expected when a short circuit arises on the stator phase. The PMSM will continue to supply energy during fault condition, the current is determined by the fault circuit. The stator inductance should be designed in such a way that the fault current is limited to the nominal current. This combined with the modular separation of each phase power circuit separates the heat distribution to a per phase problem case. This ensures that there will be no thermal damage to the windings as a result of the fault current, facilitating fault isolation. Increasing the number of phases is one way to achieve FT. A drive system has to be able to supply a rated load. For a FT machine this means it has to be able to supply the rated load whilst subjected to one fault, meaning that the remaining set of sound phases have to supply more power to compensate the faulted phase. Increasing the number of phases decreases the over dimensioning factor as one faulted phase (set) contributes less to the total.

The control subsystem is regarded separately from the converter hardware. The impact of a control approach significantly impacts the behaviour of the power converter. Different control topologies for full bridge converters can be broken down into: Direct Torque Control (DTC), Field Oriented Control (FOC), Indirect Stator Control (ISC) and Model Predictive Control (MPC) [10][20]. A study by T. Jonsky *et al.,* [10] formulated a comparison to the different classical control strategy leaving the comparison to MPC. The advantages and disadvantages proposed in this paper on the different control strategies will be applied in a later stage when comparing the candidate solution to apply on the lab setup. As for MPC, there is one drawback to this strategy: A good model has to be formulated and it requires significant

computational power [21]. This strategy can be considered superior to the alternatives should there be an infinite amount of resources to realise such a control strategy.

The control software has to be run on hardware. These MCs are also subjected to a non-zero failure probability. Another aspect to take into account is the maturity of three phase motor control. One study by Wolmarans *et al.,* [22] covered this subject and defined control partitioning in: Concentrated, modular and individual control.

2.5.1. Concentrated control

One controller generating all output signals and processing all measurements. The advantage of concentrated control is that there is a central point that governs the behaviour of the system, allowing the optimisation of the system performance. A single failure in the control unit will cause the system to stop functioning, this will effectively result in having to utilise a backup controller for redundancy. FT is not inherently in this topology due to the lack of redundancy, and has to be achieved inside a single module. This approach reduces the system complexity and avoids matching problems of multiple controllers.

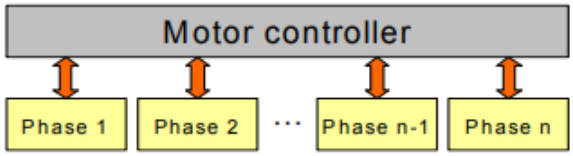

Figure 2.9: Concentrated control - Adapted version [22]

2.5.2. Modular control

Multiple controllers processing outputs and measurements for each set of phases. Modular control offers a middle ground between separation and centralised control. This strategy can be applied for multiphase machines with N sets of three phases. As it offers modularity in machine and control. A single failure will disable the faulted phase set, maintaining the remaining sound phases. Disabling more phases than necessary, as a single fault results in the inactivity of three phases reducing the available maximum output power by three times the necessary amount. This control topology seems suitable for a machine that has a large number of N-times three phases. The power reduction caused by of a single failure is mitigated by the total set of phases. For example, a six phase machine would reduce to 50% nominal power as a result of one failure whilst a twelve phase machine would be reduces to 75% of the nominal power.

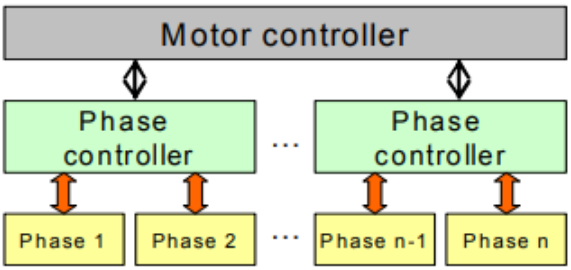

Figure 2.10: Modular control - Adapted version [22]

2.5.3. Individual control

One controller per phase, generating outputs and processing measurements for the corresponding phase. Individual control utilises the full separation of the phases but is therefore not inherently capable of optimising system performance as a whole. Asymmetric operation (in case of a fault) does not require a change in control and supports maximum available power in case of a fault. This strategy is suitable for machines that are not partitioned in many phase sets and where a FT controller has to be inherited by topology. Applying this topology will result in a more complex system that is not able to utilise radial symmetry for control.

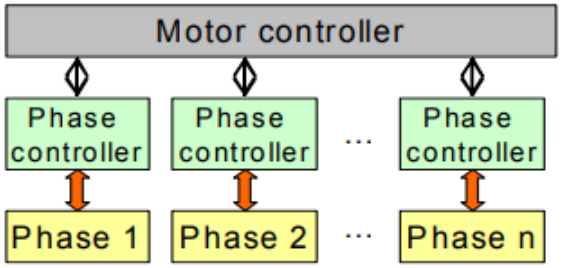

Figure 2.11: Individual control - Adapted version [22]

2.6. Sensorless rotor position determination

The function of a drive system is to translate mechanical to electrical energy and *vice versa*. This implies that the main control parameters are voltage, current, torque and speed as they govern power in both domains. Several of these attributes have to be measured in order to properly control the machine. Drive systems commonly incorporate measurements on voltage, current and speed. Utilising an encoder to measure speed will introduce a single component sensitive to failure [23]. This gives rise to the desire to determine the rotor position without encoder, as is the subject of multiple studies [24][25][26]. One additional advantage of having sensorless positioning is that the exclusion of encoders and hall sensors reduce the overall cost of the machine [26][27]. Also important to note is that the encoder is often one of the most expensive and fragile components in the drive system [26]. The implementation of sensorless control can contribute to achieving FT drive system. The determination of the rotor position without encoder can be achieved by utilising the relations in the linear circuit model of a PMSM. These equations are presented below and are formulated in the complex domain [28].

$$
\begin{aligned}
\angle\underline{\psi_f} &= \theta_r + \theta_r^0 \\
\underline{\psi_f} &= \underline{\psi_s} - L_s\underline{i_s} \\
\underline{e_s} &= \frac{d\underline{\psi_s}}{dt} = \underline{u_s} - R_s\underline{i_s} \\
\underline{\psi_s} &= \int \underline{e_s} = \int (\underline{u_s} - R_s\underline{i_s})dt \\
\underline{\psi_f} &= \int (\underline{u_s} - R_s\underline{i_s})dt - L_s\underline{i_s}
\end{aligned}
$$

This approach is subjected to non-ideal measurement of the currents and voltages. The stator parameters also vary in the case of a physical machine. This will result in inaccurate the rotor positioning depending on the application. This could result in unacceptable performance. The required rotor positioning accuracy is relatively low in standard motor applications (pumps or fans) versus high precision applications (factory robots). The determination of the stator parameters can be achieved by injecting High Frequency (HF) signals onto the stator windings, a high enough frequency will not result in significant torque contribution [25]. The advantage of this method is the possibility of determining the rotor position at low speeds.

Several approaches are presented in a review study by P. P. Acarnley *et al.,* [26]. The approaches of this study are discussed in the following paragraphs.

2.6.1. Motional EMF positioning

The first approach utilises the relation between the rotor position and the instantaneous magnitude of the EMF. Problems with this approach is in obtaining the EMF due to the rapidly changing phase current of the stator winding. A second issue with this approach is that positioning is only possible over a speed threshold. A common solution is to start with an open-loop control until the threshold speed is exceeded [26].

2.6.2. Third harmonic positioning
This approach is related to the Motional EMF position, the difference is that the third-harmonic component in the EMF waveform is utilised to determine the rotor position. This approach relies on symmetry in the three stator phases which is not always the case [26].

2.6.3. Observer based positioning
Applying an observer to a drive system is a solution to sensorless positioning from a control engineering perspective. A mathematical model of the drive system is created and supplied with the same inputs as the machine, the error is determined by comparing the output of the model to the output of the machine. The observer gives a correct representation of the system when the error is small. The drawback of this approach is that a model has to be formulated that represents the behaviour of the machine, modelling errors negatively impact the accuracy of the rotor positioning [26].

2.6.4. Induction variation
Positioning based on induction variation utilises the link between the stator current to the winding inductance and the winding inductance to the rotor position. The advantage of this approach is the ability to find the rotor position at standstill. The complexity of successfully implementing this approach is a drawback [26].

2.6.5. Flux-linkage variation
The final approach is by utilising the link between the stator voltage and current to the flux-linkage and the flux-linkage to the rotor position. This approach requires significant real-time computation power which has is becoming more easily available. Errors in determining the rotor position are described to be due to the dead-time implemented for VSC [26].

2.7. Fault probability statistics
When considering the implementation of FT in a drive system it is key to look at the type of faults that could occur and defining the probabilities. The fault types can be decomposed to originate in the machine and the converter [5][8]. Here following fault types are defined for the machine:

- Winding Open Circuit Fault (OCF).
- Winding Short Circuit Fault (SCF).

For the converter the following fault types can be defined:

- Semiconductor OCF.
- Semiconductor SCF.
- DC bus failure.

The combination of the fault types with the fault probability of a component visualises the components that need additional attention. Data provided by a study of J.W. Bennet *et al.,* [29] showed that the inverter and controller contribute to over 50% of the statistical failure chance. This was also supported in a study by J.O. Estima *et al.,* [30]. The expected failure of the machine under 5% and the estimated chance of a failure in the control signals 8%. A different study on faults in a PMSM covers a big contributor to system failures, the bearings [31].

2.7.1. Wind turbine converter data
Few studies were found that present reliability data in aerospace engineering. The studies that were found did not extensively discuss the definitions of the data. Other sources are therefore considered to analyse the reliability of drive systems. Similarities between topologies across application fields allow the use of data that is obtained from studies in other fields. A study was performed by U. Shipurkar *et al.,* [32] studying the availability of drive systems in wind turbines, presenting several parameters to the reliability of converters and categorising these rates into components. One major finding of this study is the large difference in reported failures per turbine converters per year, ranging from 0.2 to

1.32. Reasons argued for this difference is due to the choice of drive system topologies. The lower failure rate of 0.2 was found for projects that mainly utilise doubly fed IM as generators, increasing the machine failure rate but decreasing the converter failure rate due to a lower converter power rating. The rate of 1.32 converter failures per year was found for designs that incorporated mostly PMSM, reducing the machine failure rate at the cost of converter failure rate. Nonetheless, a large portion of failures originate from the semiconductor devices. The power rating of a drive system in aerospace engineering does not compare to that in wind turbines. However, it is expected that the contribution per component to the failure rate is comparable. Figure 2.12 presents a breakdown of the converter failures in the sub components [32] . The cumulative failure rate of the semiconductors (Thyristor/IGBT), inverter and control add to a 44% failure contribution, this corresponds to the claim in the previous paragraph that the expected inverter and controller failure rate contributes to 50% of the whole, making it a major contributor.

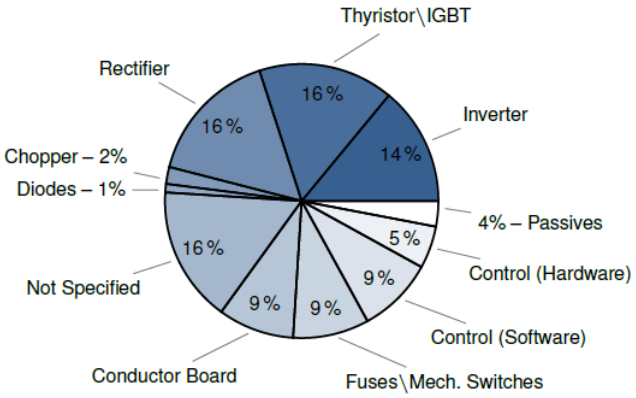

Figure 2.12: Failure rates decomposition of power converters acquired from wind turbines - [32]

2.8. Common Mode

One important aspect when considering drive systems is the CMC, especially when applying OW configurations. A study by H. Zhan *et al.,* [16] analysed the zero sequence circulating currents for PMSM, these currents are the CMC. This study identified the following sources for these disturbances:

- Machine: Zero Sequence Back-EMF.
- Machine: Cross Coupling Voltages in Zero Sequence.
- Inverter: Equivalent Zero Sequence Modulation Voltage.
- Inverter: Non-linearity.

2.8.1. Zero Sequence Back-EMF

The third harmonic component in the back-emf of PMSM is one contributor to CM problems. The cause of this back-EMF originates from the rotor magnets. The rotor field saturation often results in third harmonic distortion in the back-EMF. Manifesting itself in CMC. This contributor is also noted in a study by Y. Zhou *et al.,* [17]. This study attempts to suppress the CMV, as this is what results in circulating CMC. The intensity is determined by the magnitude of the third harmonic rotor flux density. Also stated in this study is that this CM generated by back-EMF will result in a torque ripple at six times the nominal frequency.

One advantage of this Back-EMF approach in combination with an OW common DC bus topology is the possibility to achieve sensorless rotor positioning [33]. This does not solve the problem of CMC having a negative impact on the machine. It might be possible to suppress the CMC to a minimum, reducing the negative impact but still being able to determine the rotor position by utilising this approach.

2.8.2. Cross Coupling Voltages in Zero Sequence

The cross coupling voltages between the stator phases arise when the second harmonic stator inductance is not equal to the second harmonic mutual inductance [16]. Often in contrast with a common approach in FT PMSM OW designs to apply concentrated windings with low mutual inductance. This is done to negate the effect of a faulted phase on a sound phase but in turn violate the cross coupling criteria for zero sequence voltages.

2.8.3. Equivalent Zero Sequence Modulation Voltage

This contributor on the inverter side of the system is due to the modulation strategy. One approach to modulate the gating signals is by Space Vector Pulse Width Modulation (SVPWM), resulting in triangular CM disturbance. Utilising a star connected drive system topology negates the effect of this disturbance but no longer holds for an OW approach.

3

Analysis of the existing drive system

The existing setup as currently realised has to be analysed to propose improvements. This is be done by discussing the setup according to the decomposition derived in paragraph 2.2. Certain design decisions have been made facilitating FT. This chapter will discuss how this was realised. Leaving the implementation of a control strategy that builds upon the characteristics of this design.

3.1. Machine

The machine of the setup is a modular multiphase PMSM. This machine has six stator phases that are configured as two sets of three phases (2x3). The rotor consists of eight poles and the rotor magnet is realised by applying a halbach array. The rotor design allows the assumption that the rotor field can be considered sinusoidal [1]. Table 3.1 presents an overview of nominal operating parameters of this machine.

Table 3.1: Nominal machine specifications - existing setup - [1]

Parameter	**Value**	**Parameter**	**Value**
Nominal power	50kW	Poles	8
Nominal torque	8Nm	DC-bus voltage	+/- 270V
Nominal speed	60000rpm	Stator resistance (Rs)	0.11Ω
Stator phases	6	Ld, Lq	1mH
Stator slots	12	EMF constant	0.086V/Hz

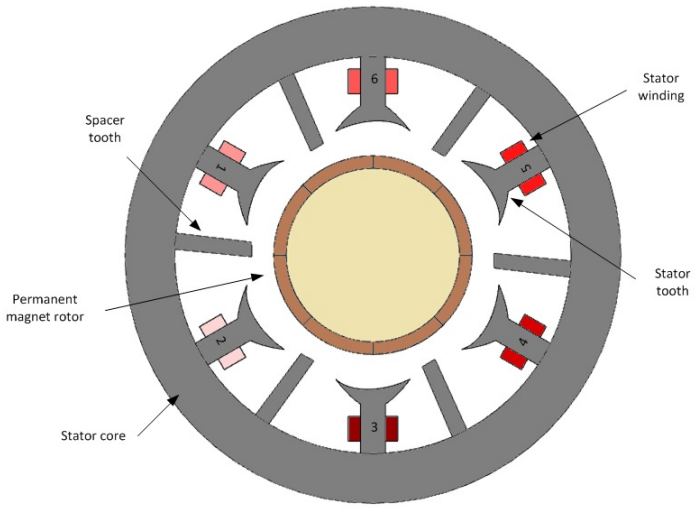

Figure 3.1: Schematic layout of the machine in the existing setup - [1]

3.2. Power converter

The power converter is designed to incorporate six H-bridge inverter modules, one per stator phase. Each switching leg consisting of four IGBT modules. These H-bridge modules are connected to a common DC bus and are isolated from ground, allowing individual control of the machine phases. The common DC bus is a single point of potential failure. Figure 3.2 visualises a graphical representation of the H-bridge converter for one set of three phases.

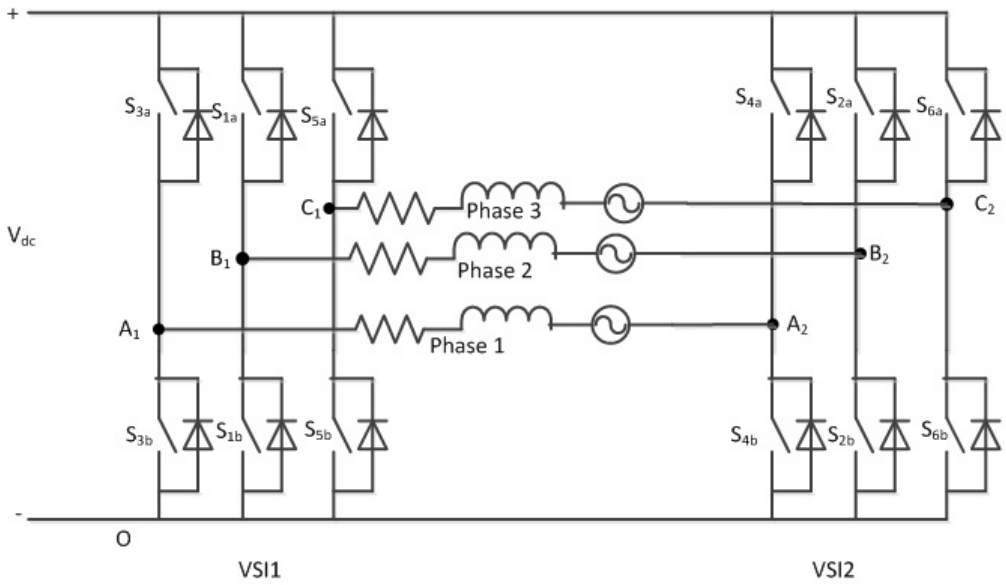

Figure 3.2: Schematic layout of an OW converter - existing setup - One set of three phases - Adapted version [1]

3.3. Control hardware

The controller is realised by partitioning in two sets of three phases. Each having a microprocessor board controlled by TI InstaSPIN, and based on FOC (TMS320F2806xF). This controller determines the rotor position in a sensorless manner by utilising an observer. At this point a master-slave control strategy is implemented. This has to be altered in order to realise FT. It is required for the slave to have input from the master controller to function, leaving a single point of system failure. An SPI communication link is also incorporated to facilitate this master-slave control strategy, also vulnerable to a single fault. When analysing the existing hardware of the existing setup it is clear that sensorless FOC modules are implemented. Therefore the argument changes whether this control method is acceptable for this project. The FOC computational effort can already be accounted for by incorporating hardware specifically designed for this control strategy. It should be taken into account not to drastically increase the computational effort when incorporating FT control. The direct current limitation is a good thing even if redundant over the stator inductance limiting the short circuit current to 1p.u. As it ensures that faults are limited below critical value. It is considered beneficial to adapt the existing sensorless FOC to incorporate FT.

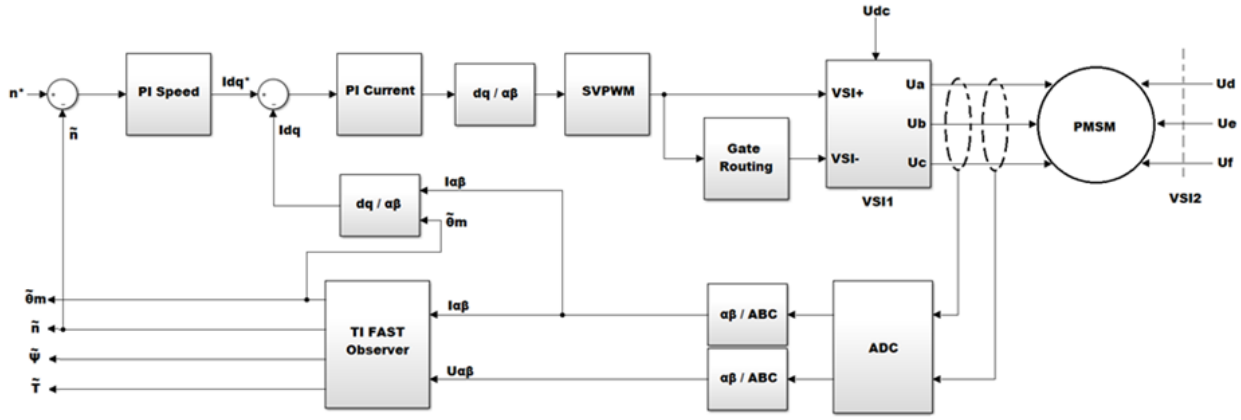

Figure 3.3: Original control system overview - Existing setup

3.3.1. SVPWM

The modulation technique applied in this setup is SVPWM. This approach relies on three phase symmetry and pre-defined space vectors. Pulses are generated by selecting space vectors that correspond to the rotor position. This does generate CMC as described in paragraph 2.8.3. A way to suppress the CMC generated by the SVPWM is by implementing phase shift based SVPWM as suggested in several studies [16][33]. Proposing an approach that is designed for OW converter systems in order to negate the CM disturbance from the inverter side. This is achieved by splitting and shifting the reference signals of the dq frame to dq1 for the left side and dq2 for the right side VSI (figure 3.4). Visualised here is the transformation matrix equation and the vector representation. The reference voltage is recreated as a linear combination (LC) of the left and right side inverter signals.

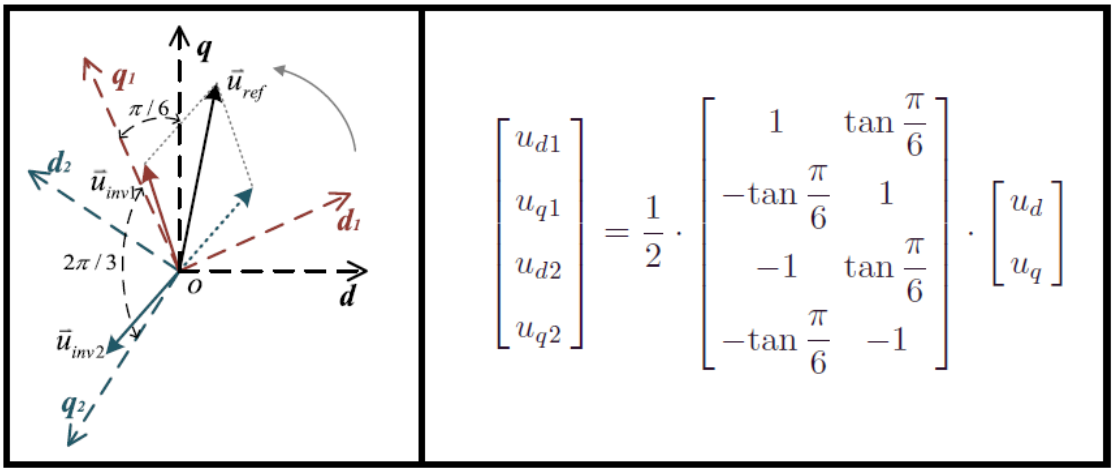

$$\begin{bmatrix} u_{d1} \\ u_{q1} \\ u_{d2} \\ u_{q2} \end{bmatrix} = \frac{1}{2} \cdot \begin{bmatrix} 1 & \tan\frac{\pi}{6} \\ -\tan\frac{\pi}{6} & 1 \\ -1 & \tan\frac{\pi}{6} \\ -\tan\frac{\pi}{6} & -1 \end{bmatrix} \cdot \begin{bmatrix} u_d \\ u_q \end{bmatrix}$$

Figure 3.4: Phase shift SVPWM graphical representation and transformation matrix - Adapted version [33]

3.4. Drawbacks

The existing drive setup is a work in progress. At this point it is able to operate according to the initial design. The hardware is designed to facilitate FT but is not yet incorporated in the control system. Several items are formulated that have to be resolved to achieve a FT drive system.

- The machine has only been tested in no-load condition, in order to validate the existing control system a loaded test should be performed.
- A master-slave controller strategy and the common DC bus is in contrast to the goal of FT.

- The SVPWM strategy results in CMC, this has to be reduced.
- The black-box nature of the MC board could lead to problems when attempting to operate the system in faulted condition.
- It is unknown if the TI FAST observer is capable to determining the rotor position in post-fault condition.

3.5. Simulation model

A model was constructed previous to the start of this thesis. This model consisted of a three phase representation of the drive system as realised in the existing setup [1]. This section will discuss the working of this model and will present the performance of the system. The contribution to the original model is done by realising the expansion to a dual three phase system and ability to introduce an OCF. This model consists of four subsystems discussed in the following paragraphs and are categorised as: Machine electrical, machine mechanical, power converter and control system.

3.5.1. Power Converter

The power converter is modelled as an H-bridge converter as realised in the existing existing setup. A figure of a single phase module is visualised in figure 3.5. The DC bus connection is supplied by an ideal DC source (45V). Gate signals originate from the control system. Four IGBT modules are utilised from the Matlab Simulink library. The load is represented by a voltage controller current source.

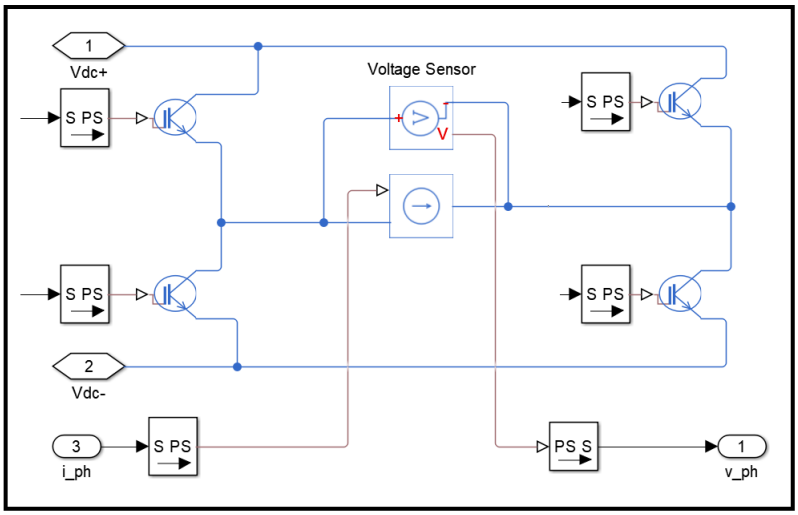

Figure 3.5: Power converter module (single phase) - Matlab Simulink

The IGBT modules in the Matlab Simulink library are a reasonable approximation for the existing setup, as these are not ideal switches. The parameters of the IGBT are visualised in table 3.2. The expected result of modelling the switches in semiconductor components is the contribution to the CM disturbance. The IGBT switching module consist of an IGBT switch and an internal reverse diode. There is a difference between the IGBT and the diode forward voltage drop. This will result in asymmetry between the stator phases which results in CMV, this results in circulating CMC.

Table 3.2: Parameter settings for the IGBT modules in Matlab Simulink

Parameter	IGBT	Diode
Forward voltage (V)	1.2	0.8
On resistance (Ohm)	1e-3	1e-3
Off resistance (Ohm)	1e-5	1e-5
Threshold voltage (V)	6.0	-

The load is modelled in combination by the DE (Differential Equations) of the machine electrical subsystem. By imposing the terminal voltage on the machine electrical subsystem and computing the current. This current is then returned and imposed to the controlled current source.

3.5.2. Machine electric model

The machine is divided in an electrical and a mechanical part for this model. The overall model of the machine electrical subsystem is visualised for a single phase in figure 3.6. The input of this subsystem is the voltage of the power converter and the electrical rotor angle corresponding to the phase. The output of this subsystem is the current that flows back to the power converter and the generated torque (Te).

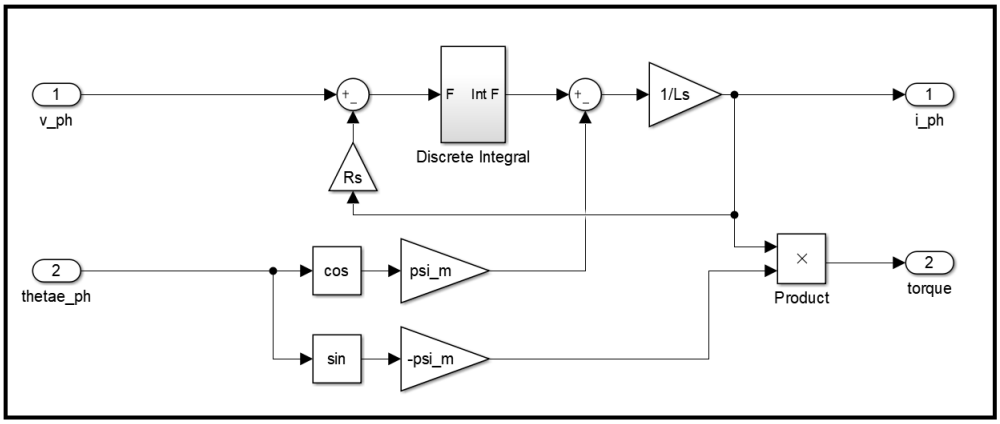

Figure 3.6: Electric machine module (single phase) - Matlab Simulink

As previously mentioned the machine model is based on the DE of a single machine phase. The following equation is therefore similar to the model as portrayed in figure 3.6 (equations in continuous time).

$$T_e = \sum_{n=1}^{6} \underline{i_n} \cdot -\psi_m sin(\theta_n)$$

$$\underline{i_n} = \frac{1}{L_s} \int_{t=t_0}^{t_e} (\underline{u_n} - R_s \underline{i_n} dt - \psi_m cos(\theta_n)) dt$$

3.5.3. Machine mechanic model

The model of the mechanical part of the machine is visualised in figure 3.7. This subsystem translates the torque input from the electrical subsystem to speed and electrical angle(s). The electromagnetic torque (Te) and load torque (Tm) determine the resulting torque load on the rotor, allowing the computation of the rotor speed. Integrating the angular rotor frequency translates to the rotor angle. The function subsystem is placed to correct the load for Clockwise (CW) and Counterclockwise (CCW) rotation. In motor applications the determination of the rotor position is normally done by an encoder, this model assumes that the position can be determined. The model for this subsystem can also be described by utilising DE. These equations represent the computation in this model (in continuous time).

$$T = Te - Tm$$

$$\omega_m = \int_{t=t_0}^{t_e} \frac{T}{J} dt = \frac{d\theta_m}{dt}$$

$$\theta_e = p\theta_m$$

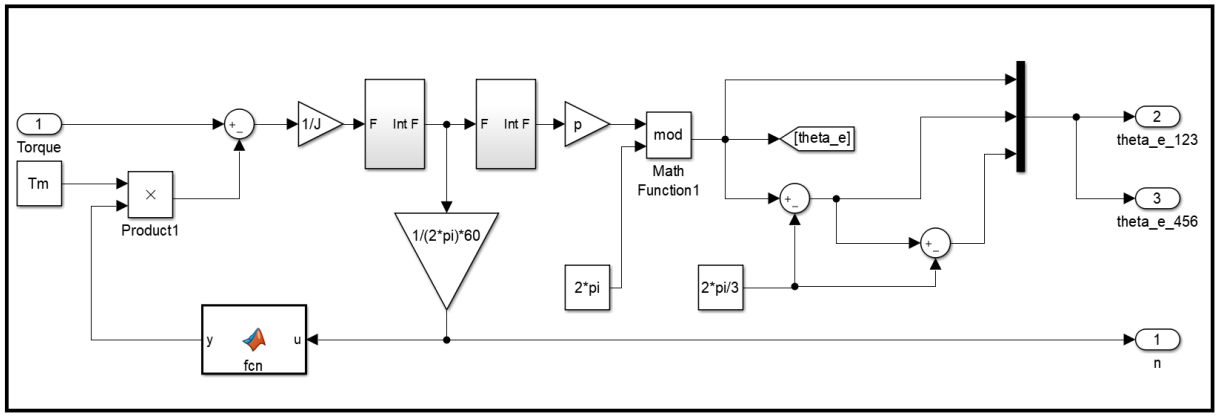

Figure 3.7: Machine mechanical model - Matlab Simulink

3.5.4. Control system

The final subsystem to be discussed in this chapter is the control subsystem. This system can be divided in three modules: PI speed, PI current and SVPWM. The combination of speed and current control is a commonly used cascade control technique. The output of the speed controller is directly coupled to the q-axis input of the current controller. This is the current contributing to torque. The d-axis is set to zero for this model as it does not contribute to torque. This thesis focuses on the functioning of the machine, there is no need to consider controlling the d-axis current.

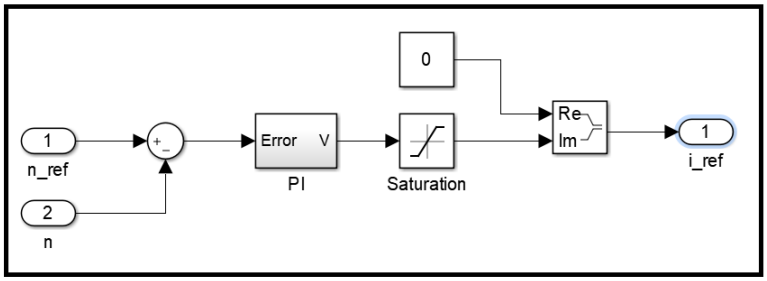

Figure 3.8: Controller model - PI speed - Matlab Simulink

The current controller controls the d and q input from the speed controller in two separate PI controllers. In order to do so the measured phase currents have to be transformed from abc to dq coordinates. Applying saturation ensures that the physical limitations of the power converter is respected. The output of this controller is the voltage in AlphaBeta coordinates. The VSI output is a Pulse Width Modulation (PWM) voltage waveform, the current is a result of that voltage waveform.

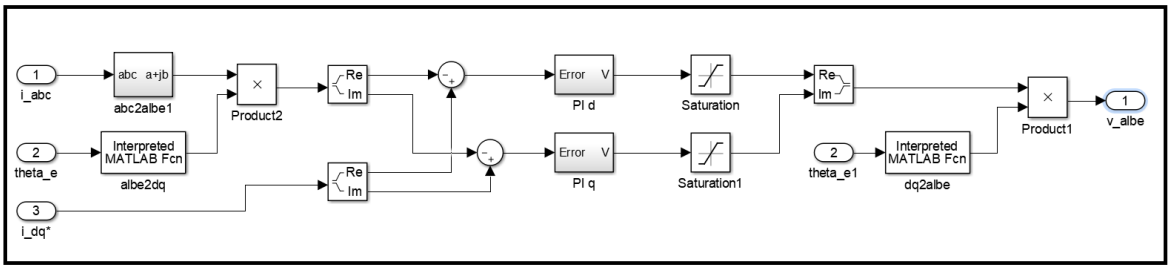

Figure 3.9: Controller model - PI current (DQ) - Matlab Simulink

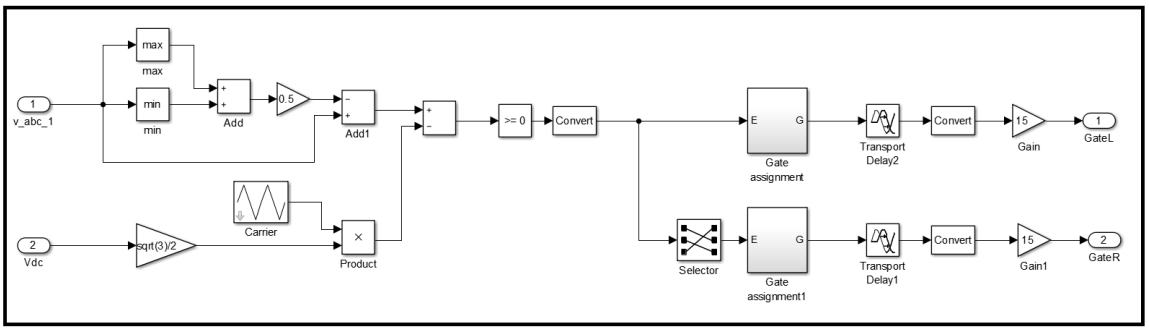

Figure 3.10: Controller model - SVPWM - Matlab Simulink

Table 3.3: Settings of the PI controllers - Matlab Simulink

Controller constant	Speed	Current
Kp	2	6
Ki	100	660

4

OW machine control with CM suspension

Chapter 2 concluded with a discussion on CM disturbance. This disturbance was observed in the existing setup, and has a triangular waveform [1]. The origin of this disturbance is expected to be due to the SVPWM technique, as discussed in paragraph 2.8. This chapter will first present the response of the simulation model of the existing setup. Simulations will show if the CMC observed in the simulation is also triangular. A new control system will be formulated and implemented. A comparison of system behaviour will determine if the new control system adds value with regard to FT.

4.1. Original system response

The following paragraphs will cover the original system behaviour in pre- and post-OCF condition. The functioning of the machine is observed by analysing the torque and speed. The current and CMC will be presented, as it is aimed to improve these parameters whilst retaining functionality. The tested scenario in this study is a case similar to the tests performed in the previous study [1]. The speed refers to the 50Hz equivalent when considering eight rotor poles. The DC bus voltage were set at a safe level. The original tests was performed without loading the machine, a mechanic load was included in the simulation to visualise the CMC during operating conditions.

Table 4.1: Operating scenario parameters

Parameter	Value
Speed (rpm)	750
Mechanic load (Nm)	0.2
DC bus (V)	45

Figure 4.1 and 4.2 presents an overview of the original system response. Several time periods are displayed in this figure. The first time period is the start-up, during this period the rotor accelerates to the reference speed. This period is followed by a (pre-fault) steady state period. The rotor speed settles at the reference speed due to the integral action of the PI controller. An OCF (phase 4) is introduced at 0.2 seconds followed by a post-OCF steady state condition. The final period is the dynamic response in post-OCF condition. This is simulated by increasing the speed reference by 10%.

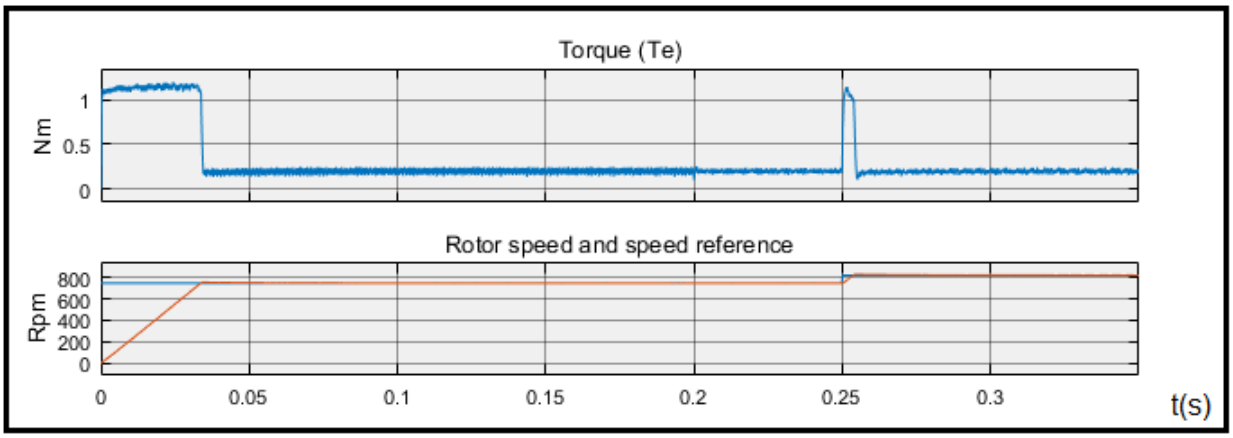

Figure 4.1: Original system response - Mechanic overview

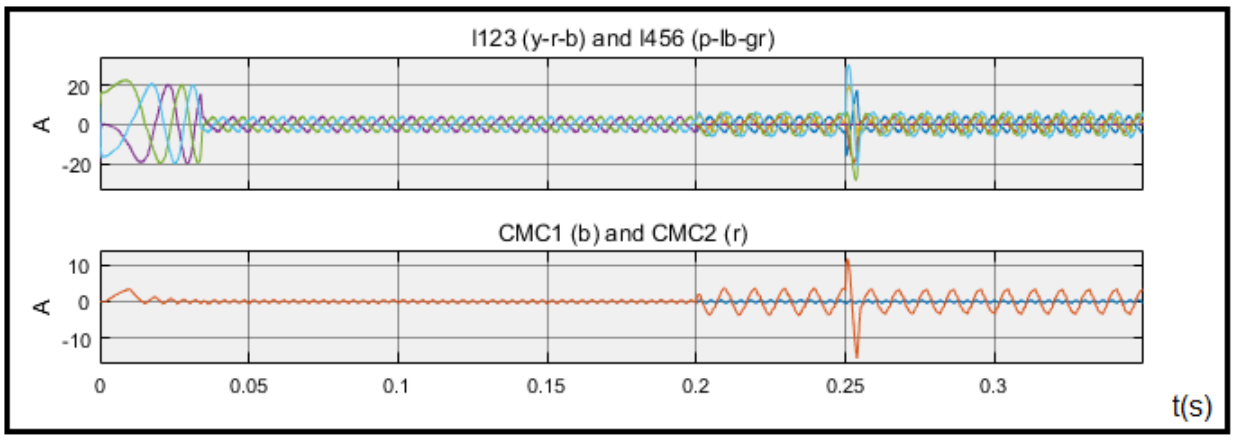

Figure 4.2: Original system response - Electric overview

4.1.1. Original system behaviour - Start-up

The start-up period is investigated in this subsection. A close up of the start-up period is presented in figure 4.3 and 4.4. The start-up shows smooth acceleration with a settling time (ts 2%) at roughly 0.03 seconds. A slight overshoot occurs and is not well visible in the figure. The rotor speed then approaches the reference signal as expected due to the integral action of the PI controller. Figure 4.4 shows the stator currents and CMC during the start-up period. Noticeable in this graph is the large CMC in the first cycle of the stator current. The CMC decreases as the rotor speed increases.

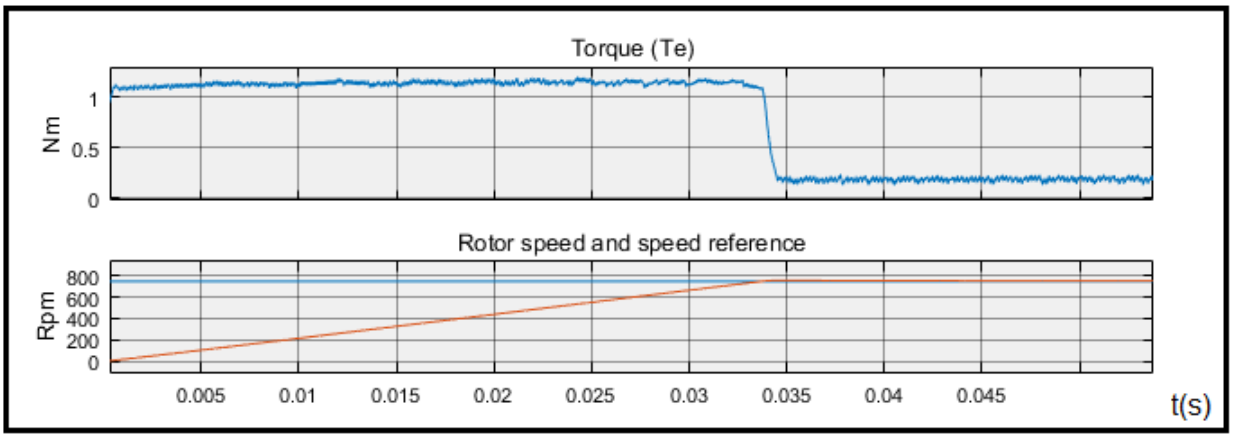

Figure 4.3: Original system response - mechanic start-up

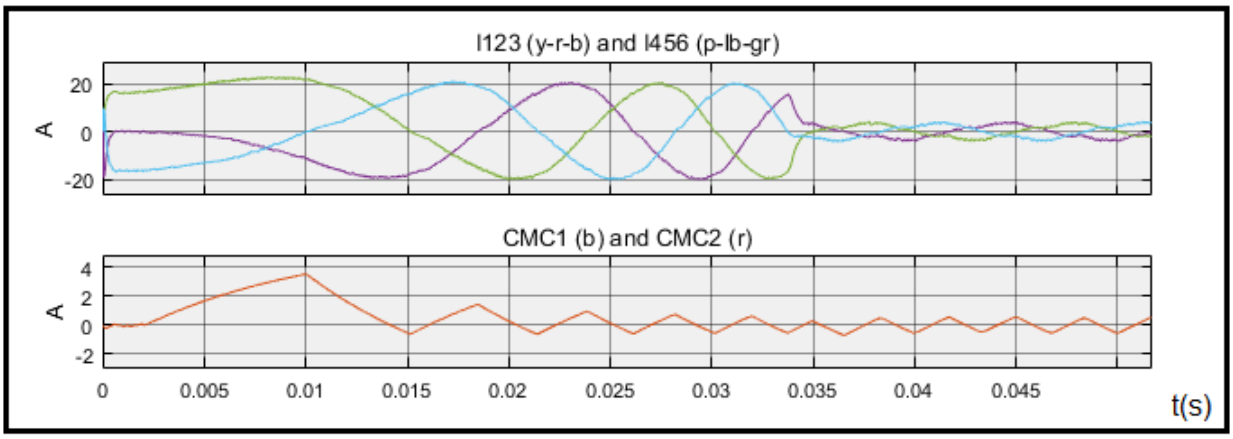

Figure 4.4: Original system response - Electric start-up

4.1.2. Original system behaviour- Steady state

This subsection will focus on the steady state period following the start-up. The mechanic and electric behaviour is visualised in figure 4.5 and 4.6. The CMC of phase set 1 (1, 2 and 3) is the same as for phase set 2 (4, 5 and 6). The triangular waveform is observed as expected [16]. This CMC is described to be of non issue in star connected topologies. However, for an OW topology this is not the case. These currents will circulate between the positive and negative side of the converter.

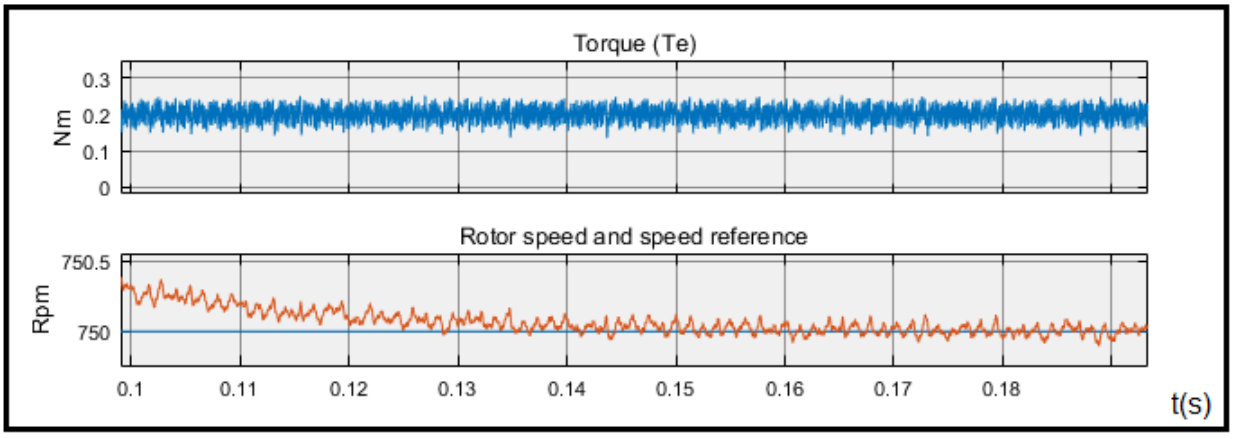

Figure 4.5: Original system response - Mechanic steady state

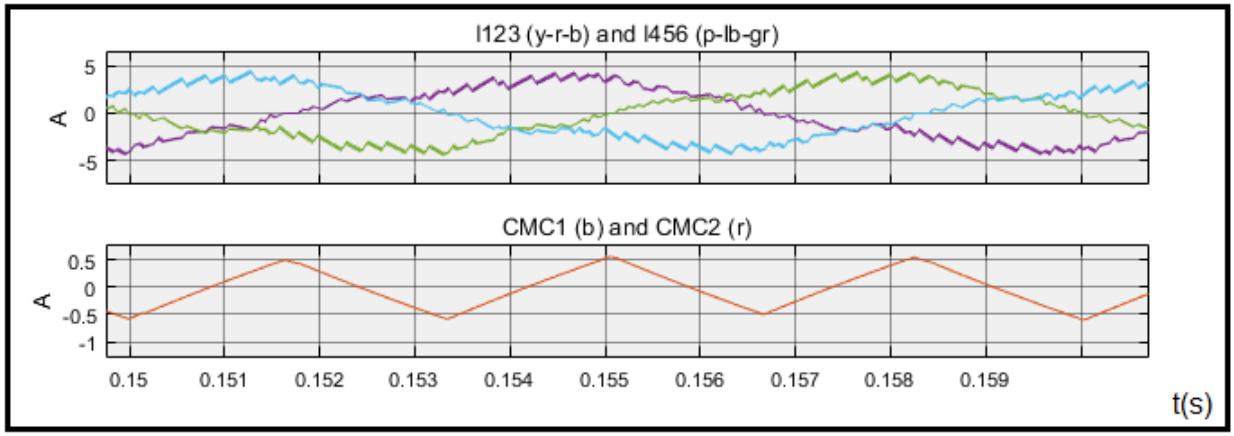

Figure 4.6: Original system response - Electric steady state

4.1.3. Original system behaviour - Post-OCF

The impact of an OCF in this drive system will normally result in one phase set being unable to function. The other phase set will therefore have to supply the load. This means that the machine has to be oversized or that the post-OCF load has to be reduced. This thesis aims to provide a solution to continue operation with the remaining (five) phases when subjected to a fault. This increases the post-OCF nominal power of the system in an asymmetrical configuration. The OCF is simulated and the results are presented in figure 4.7 and 4.8. The fault will force the voltage and current of phase 4 to zero, the rest of the system is left unaltered.

The results show that the mechanic performance is not affected in any significant way due to the OCF. The current is distorted in the remaining phases. The lack of radial symmetry can be observed in CMC2, this current has an amplitude close to the phase current. In order to formulate a solution to the existing system it is argued that the CMC has to be reduced both pre-fault and post-OCF. This has to be achieved whilst maintaining acceptable torque.

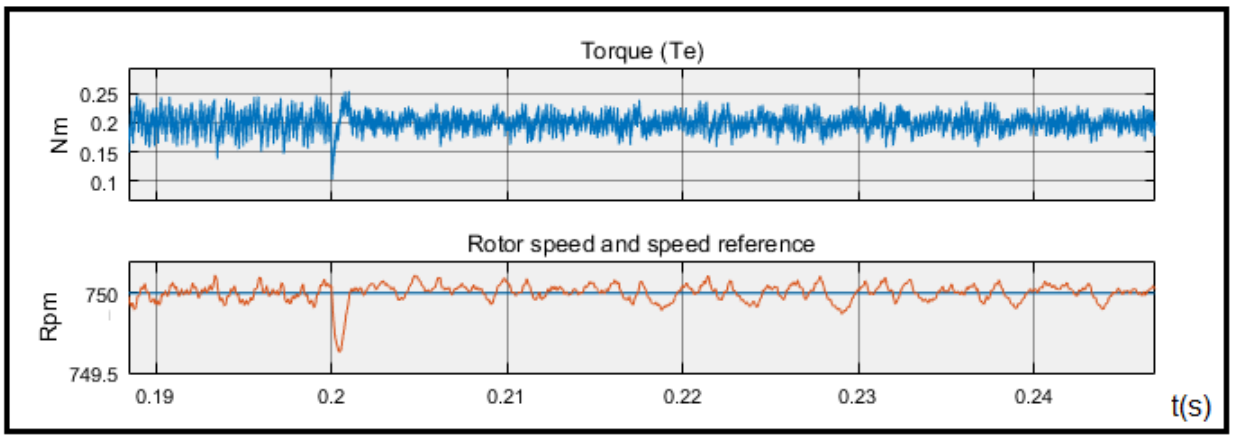

Figure 4.7: Original system response - Mechanic post-OCF

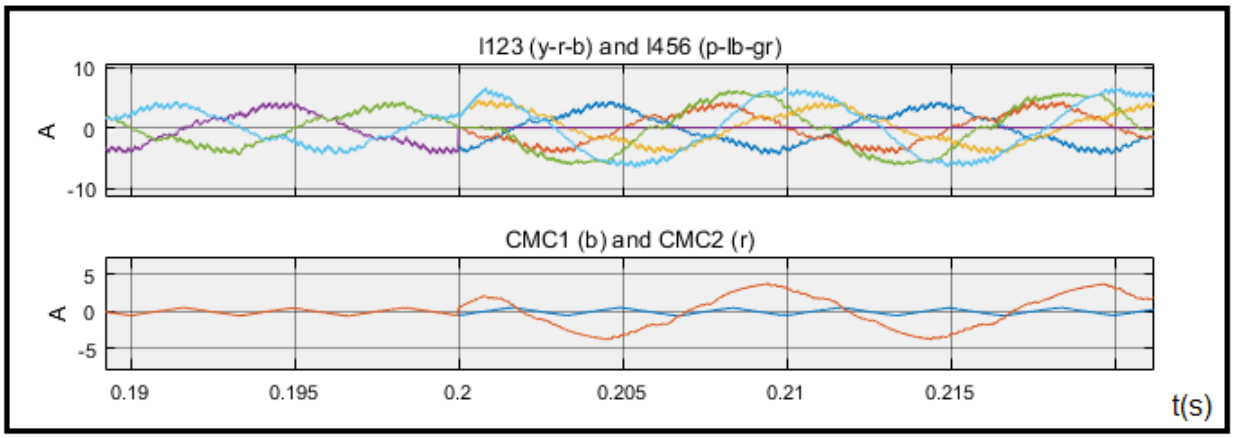

Figure 4.8: Original system response - Electric post-OCF

It is also aimed to show the post-OCF dynamic performance of the drive system in this simulation. This is achieved by increasing the speed reference by 10% at 0.25 seconds, during the post-OCF period. The results of this test are visualised in figure 4.9 and 4.10. The system is capable to perform under dynamic conditions, the stator current and CMC does increase drastically during acceleration.

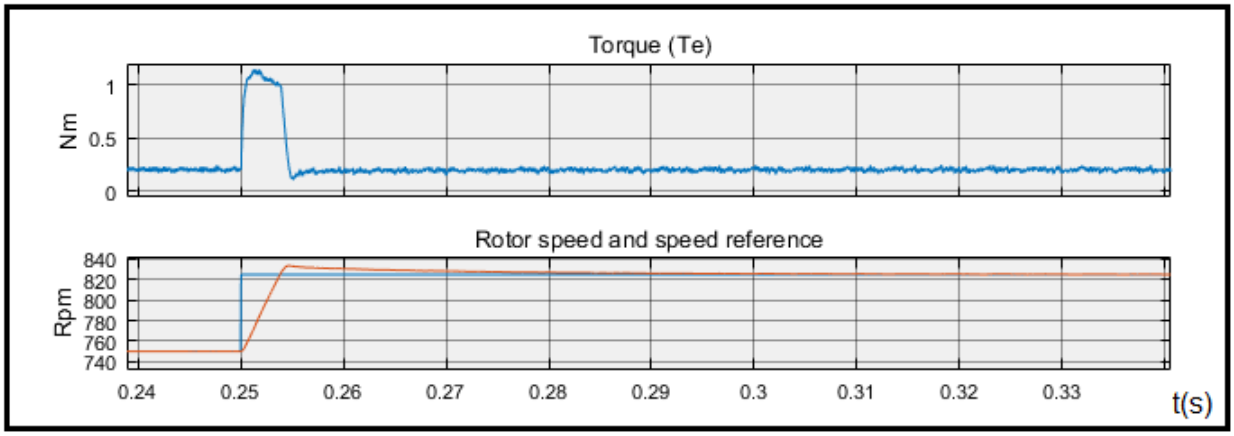

Figure 4.9: Original system response - Mechanic post-OCF - Dynamic

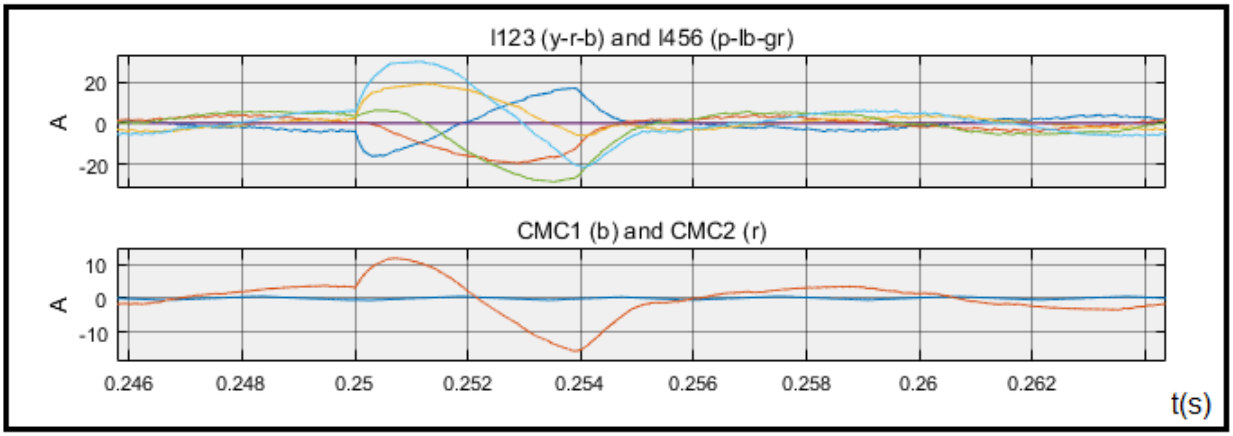

Figure 4.10: Original system response - Electric post-OCF - Dynamic

4.2. CM current suspension

This section will focus on the new control system that aims to improve the system performance. The control system will be applied to the existing hardware. The main aspect is the reduction or elimination of the CMC. Several approaches from literature were presented in the literature study (chapter 2), none of these cover post-OCF operating conditions. An approach has to be formulated that allows successful FT implementation in post-OCF condition.

4.2.1. DQ0 control

Literature presents two approaches to control the CMC. The first is by pre-defining the space vectors that contribute to the CMV, leading to CMC. The second is by actively controlling the zero sequence. The vector approach relies on the availability of the space vectors, this is considered to complex to apply for post-OCF conditions. The approach to implement active dq0 control is the primary candidate to reduce the CM disturbance.

One study formulating an active dq0 control for OW topologies is proposed by Y. Zhou *et al.*, , [17]. The principle of this approach is by redistributing the zero space vector. The reference vector is constructed as a LC of two space vector states and then reduced by introducing the zero vector. There are to possibilities to realise zero voltage: V0 (000) and V7 (111). These two vectors are usually split evenly to assure a balanced use of the IGBT modules, this control room is utilised to control the CMV. Figure 4.11 and 4.12 visualise the principle to implement this approach. The space vectors are formulated in combination with CMV. The control room is the distribution between V0 and V7. Both vectors result in a zero, with different CMV. Redistributing the zero state across V0 and V7 will generate a CMV between 0 and Udc on average. The open end winding allows the negative converter side to modulate the CMV between 0 and -Udc. The issue with this approach is that the modulation index impact the control room, the amount of CMV that can be controlled is proportional to the available zero time. Building upon this idea it is believed that the redistribution of the zero vector still holds in post-OCF condition. Especially when considering that the setup analysed in this project consists of twice the phases and inverter modules compared to the example [17].

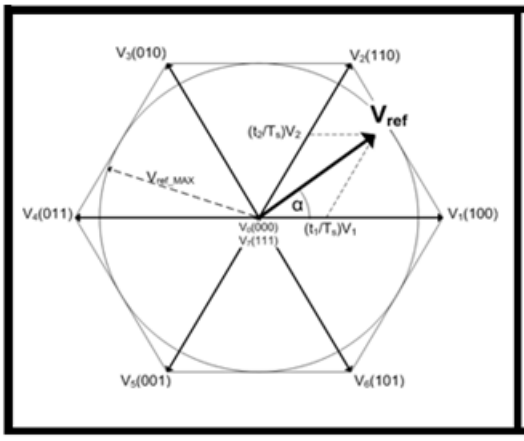

	Vector	Switch state	Value	CMV
Zero vectors	V_0	(000)	0	0
	V_7	(111)	0	U_{dc}
Active vectors	V_1	(100)	$2U_{dc}/3$	$U_{dc}/3$
	V_2	(110)	$U_{dc}/3+j\sqrt{3}\,U_{dc}/3$	$2U_{dc}/3$
	V_3	(010)	$-U_{dc}/3+j\sqrt{3}\,U_{dc}/3$	$U_{dc}/3$
	V_4	(011)	$-2U_{dc}/3$	$2U_{dc}/3$
	V_5	(001)	$-U_{dc}/3-j\sqrt{3}\,U_{dc}/3$	$U_{dc}/3$
	V_6	(101)	$U_{dc}/3-j\sqrt{3}\,U_{dc}/3$	$2U_{dc}/3$

Figure 4.11: SV switching vectors with corresponding CMV - Figure:[34], CMV:[17]

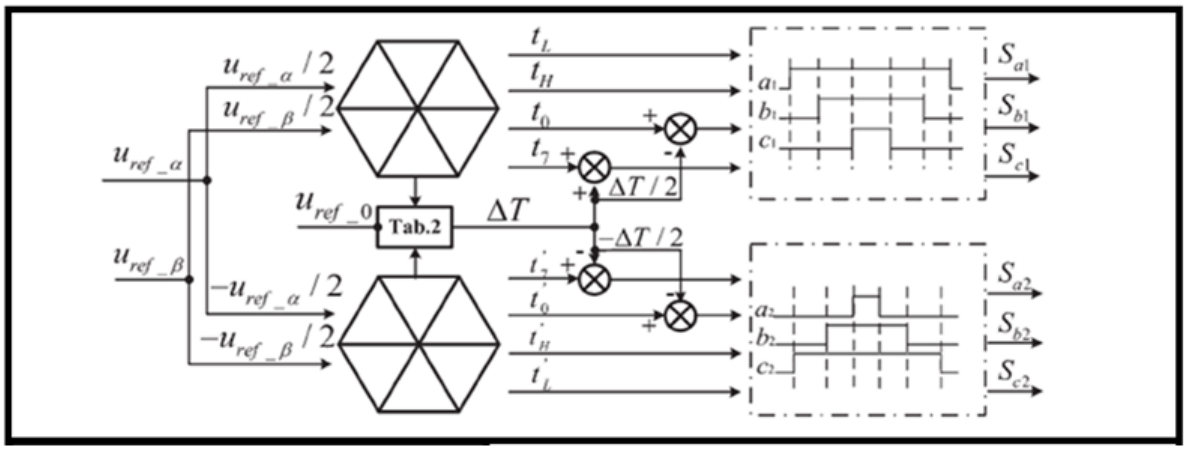

Figure 4.12: Control schematic on implementing the redistribution of the zero vector [17]

4.2.2. Model implementation

The implementation of the control strategy formulated [17] is done by expanding the current control from dq to dq0. Adding a Proportional Resonant (PR) controller for the zero sequence current and by replacing the SVPWM by the Zero Voltage PWM (ZVPWM) subsystem. One thing to note is that the Common Mode Reduction (CMR) control strategy was concerned for a machine with three phases. The difference with the setup of this project is that there are six stator phases. Therefore there will be a total of four converters following the definition in literature [17]. Combining the zero sequence control for the VSI sets was considered, due to the desire for FT it is argued that a total split between the two sets of stator phases is the logical approach. Table 4.2 presents the control constants for the PR controller. The factor for the resonant controller (Kr0) is set to zero. The inclusion of this factor is to correct for the 3rd harmonic component in the back-emf that often occurs in PM machines. The rotor field is ideally perfectly sinusoidal due to the application of a halbach array, the resonant control is not required in this case.

Table 4.2: Settings of the PI controllers - Matlab Simulink

	Speed	**Current (dq)**	**Current (0seq)**
Kp	3	20	10
Ki	75	2200	-
Kr	-	-	0

Figure 4.13 shows a schematic overview of the CMR control strategy. This figure shows the PI control for the dq axis and an expansion of a PR controller for the zero-sequence. The delta components are added to the controller as well and are calculated by the equations below. Including the zero sequence is not necessary for the existing drive setup. The application of a halbach array leads to a sinusoidal rotor field, the third harmonic is therefore nonexistent.

$$\Delta U_d = \omega L_q i_q$$
$$\Delta U_q = \omega \Psi_r - \omega L_d i_d$$
$$\Delta U_0 = 0$$

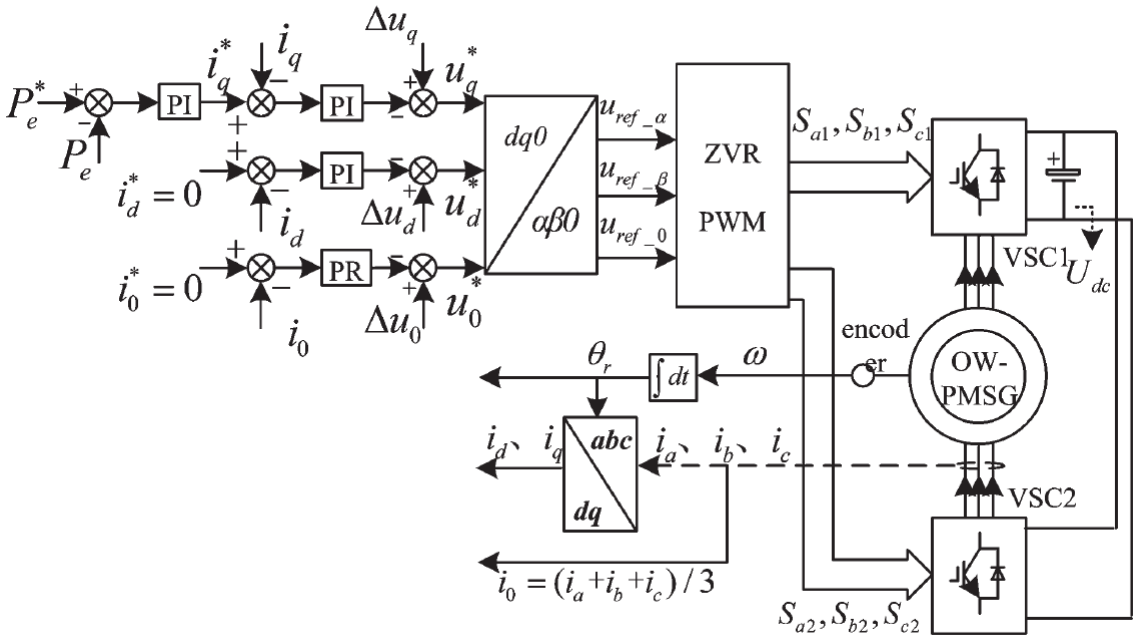

Figure 4.13: Schematic overview and vector diagram of the (dual) OW converter [17]

4.2.3. ZVRPWM

ZVRPWM is performed by distributing the switching modes over the sampling time (Ts). The switching times are then allocated to the correct phases by the argument of the reference voltage. The reference voltage in the alphabeta reference frame is normally represented in cartesian coordinates in the complex plane, transforming to polar coordinates presents the modulus and the argument.

$$\underline{U^*_{\alpha\beta}} = U^*_\alpha + jU^*_\beta = re^{j\phi}$$

The modulus of the reference signal leads to the determination of the modulation index. This index is determined by the modulus of the reference signal and the DC bus voltage.

$$m = \frac{r}{U_{dc}\frac{2\sqrt{3}}{3}}$$

Six sectors are defined for the dual converter, the argument of the reference signal represents the angle in the complex plane. This angle is used to determine the sector. Three time quantities are defined [17] and presented in the equation below. These constant represent the active vector time. The sector determines the routing of these parameters to the phases.

$$X = T_s m \cdot sin\phi$$
$$Y = T_s \frac{\sqrt{3}m \cdot cos\phi + m \cdot sin\phi}{2}$$
$$Z = T_s \frac{-\sqrt{3}m \cdot cos\phi + m \cdot sin\phi}{2}$$

Table 4.3 presents the routing of the vector time parameters to the switching time periods (TL and TH). These sectors are defined by angle thresholds presented in in figure 4.14. The model implements the determination of the sector by a compactor operation between the argument of the reference signal to the pre-defined sector angles. TL represents the dwell time of the active vector that modulate the CMV to Udc/3, TH represents the modulation to 2Udc/3. The CMV contribution was previously presented in figure 4.11.

Table 4.3: Dwell time allocation [17]

Section	TL	TH
I	-Z	X
II	Z	Y
III	X	-Y
IV	-X	Z
V	-Y	-Z
VI	Y	-X

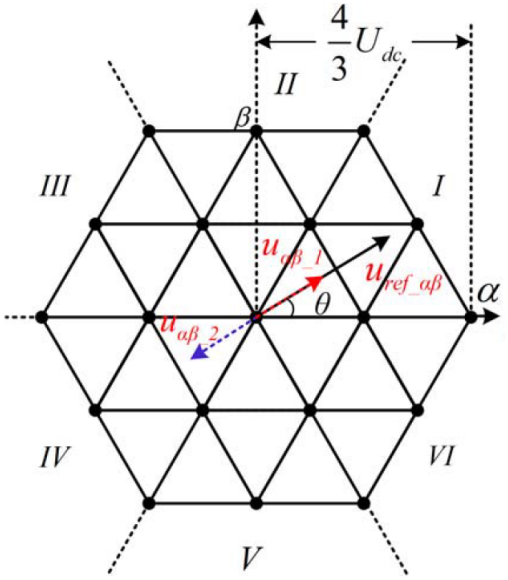

Figure 4.14: Sector definition of the CMR control strategy [17]

The zero mode is normally distributed evenly between V0 and V7, this is not the case when redistributing for zero sequence control. The redistribution parameter is described in the equation below. This is the point where the zero sequence reference voltage is included.

$$\Delta T = \frac{T_s U_0^*}{U_{dc}} + \frac{T_L - T_H}{3}$$

The following equations described the redistribution for V0 and V7. The zero time is determined by the switching period and the active period. The tilde represents the original (even) distribution of the zero vector. The redistribution parameters is added to determine V0 and V7.

$$\begin{aligned} \widetilde{T_0} + \widetilde{T_7} &= T_s - T_L - T_H \\ \widetilde{T_0} &= \widetilde{T_7} \\ T_7 &= \widetilde{T_7} + \Delta T \\ T_0 &= \widetilde{T_0} - \Delta T \end{aligned}$$

The previous equations were formulated for the left side switching legs. The zero vectors for the right side (T') switching legs are mirrored to the left side (T).

$$\begin{aligned} T_0 &= T_7' \\ T_7 &= T_0' \end{aligned}$$

The time vectors (TH, TL, T7 and T0) are then converted to duty cycles. This allows the construction of pulses.

$$T = DT_s$$

The implementation of the ZVRPWM is visualised in figure 4.15. The subsystem blocks in this figure represent the equations formulated in this paragraph. This figure presents the ZVRPWM process for the left side switches of one of the OW converter modules. There are a total of four identical modules in the simulation model.

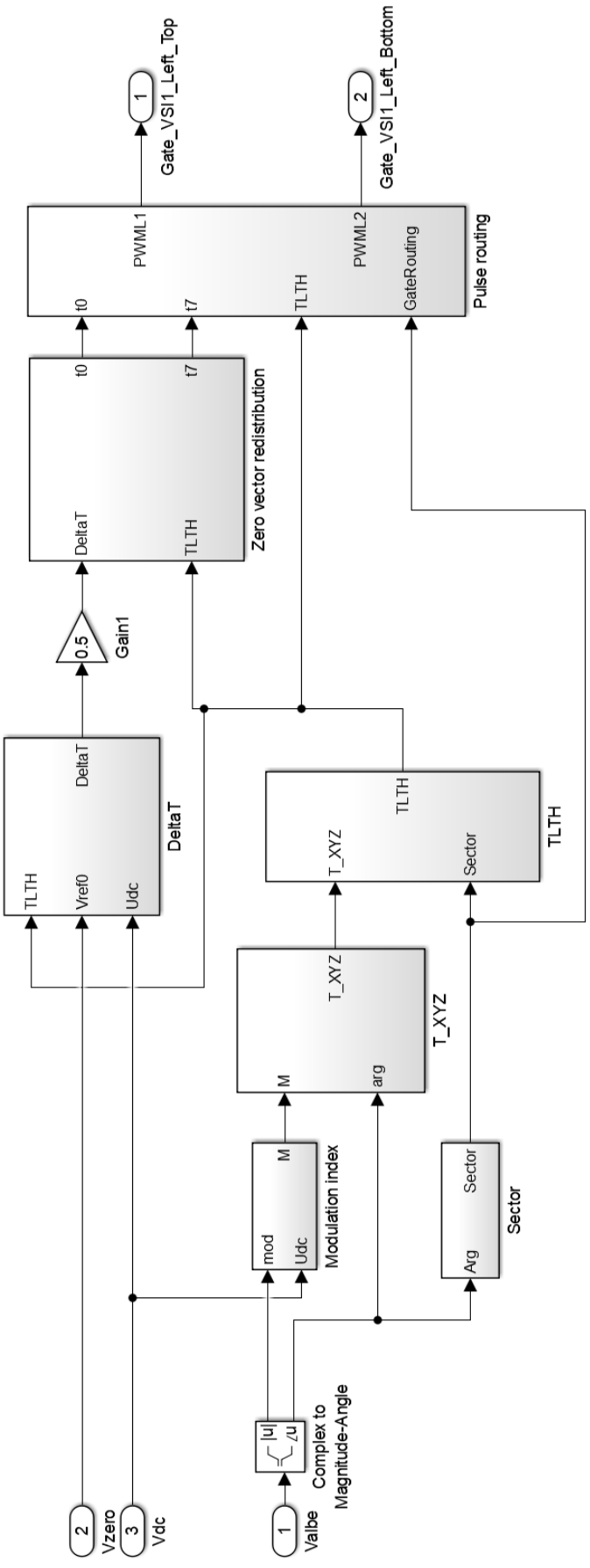

Figure 4.15: Matlab Simulink model implementation of ZVRPWM

4.2.4. Pulse centering

When implementing the model it is found that it not straightforward to implement a centred pulse in the sampling period. Implementing the PWM in the model relied on achieving centered pulses with respect to the sampling period. Left and right side aligned pulses are simple to realise, an approach to construct a centered pulse out of left and right side pulses is implemented. In practice a left aligned pulse can be implemented by applying a comparator with a saw-tooth waveform, this can also be done to a right side pulse. A left side pulse function is defined as P(D), a right side aligned pulse function is defined as the inverse P(-D). The equation below formulates how to construct a centered pulse by utilising left and right side aligned pulses. This equation was successfully tested separately to validate the working. Saturation was applied to limit the input between 0 and 1. The correct pulses are also generated in the limit cases where the desired duty cycle is equal to 0 or 1. One example on the implementation of this equation is presented in the second equation below and visualised in figure 4.16. A desired duty cycle of 0.6 is imposed in this equation. The left and right side pulse therefore have a duty cycle of 0.2. Subtracting the left and right side pulse from the unit pulse with duty cycle 1.0 will result in the desired centered duty cycle.

$$P_{centre}(D) = 1 - P_{left}(\frac{1-D}{2}) - P_{right}(\frac{1-D}{2})$$

$$P_{centre}(0.6) = 1 - P_{left}(\frac{1-0.6}{2}) - P_{right}(\frac{1-0.6}{2})1 - P_{left}(0.2) - P_{right}(0.2)$$

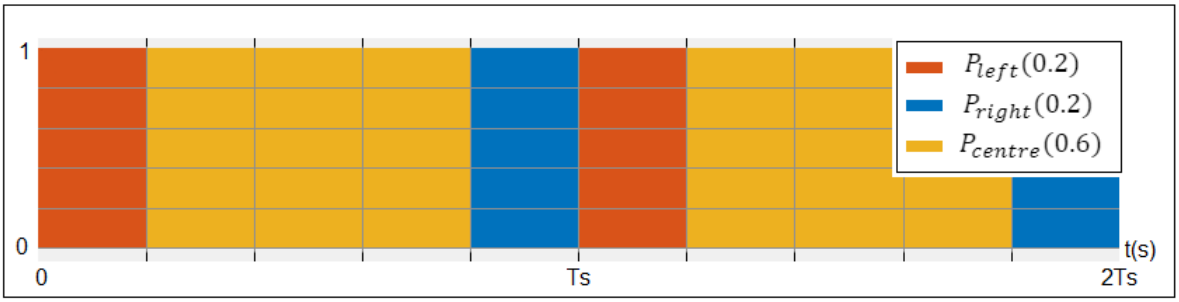

Figure 4.16: Example that visualises the pulse centering principle for desired duty cycle D=0.6

4.2.5. Inclusion of dead time

One aspect that was not modelled in the original simulation was dead time. Dead time is implemented in the VSI control to ensure that there is no overlap between the top and bottom switch, as overlap will result in a short circuit. This does increase the CM disturbance. The implementation of dead time was done be expanding upon the pulse centering subsystem. The approach is described in the equations below and is visualised in figure 4.17. The reduction in duty cycle to incorporate the dead time was divided evenly between the positive and negative pulse. To ensure that as much symmetry will be observed as possible, any asymmetry will result in CM disturbance.

$$D_{old}^{down} = 1 - D_{old}^{up}$$
$$D_{new}^{up} = D_{old}^{up} - \frac{Dtd}{2}$$
$$D_{new}^{down} = D_{old}^{down} + \frac{Dtd}{2}$$

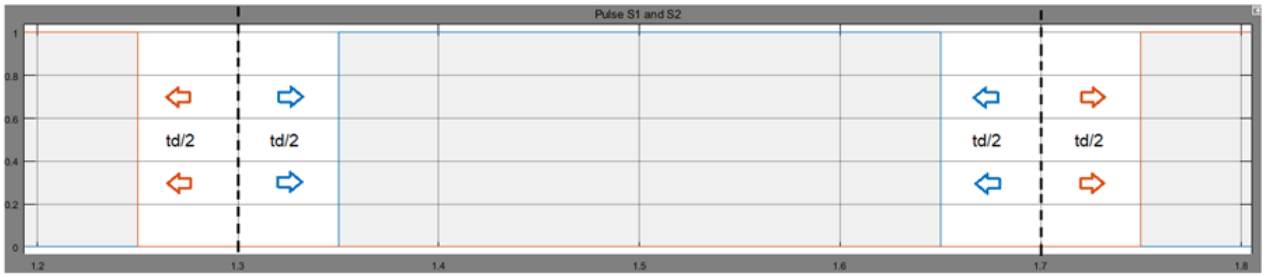

Figure 4.17: Dead time implementation as applied symmetrically

4.3. CMR system behaviour

The following paragraphs will analyse the CMR system response in a similar approach to the original system response (section 4.1). The operating condition is also equal to the original simulation. Figure 4.18 and 4.19 presents an overview of all time periods. The first observation is that the rotor speed follows the reference speed. The second observation is that the CMC is not severely affected during post-OCF conditions.

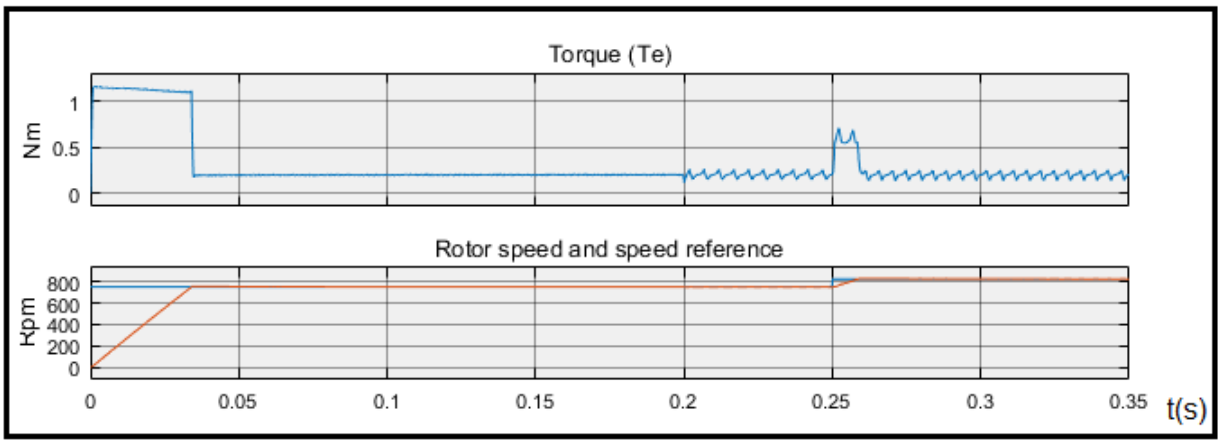

Figure 4.18: CMR system response - Mechanic overview

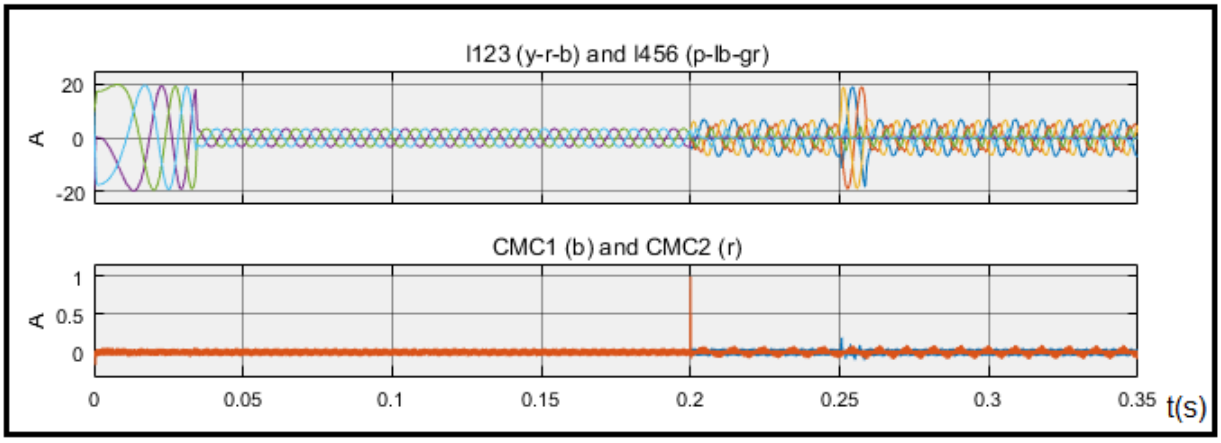

Figure 4.19: CMR system response - Electric overview

4.3.1. CMR system behaviour - Start-up

The start-up period is visualised in figure 4.20 and 4.21 for the mechanic and electric behaviour respectively. Comparing the CMR system to the original shows more ripple in the torque. It also shows that the rotor speed approaches the reference speed slightly later at roughly 0.03 seconds (ts 2%). The magnitude of the CMC remains constant during the start-up and steady state period.

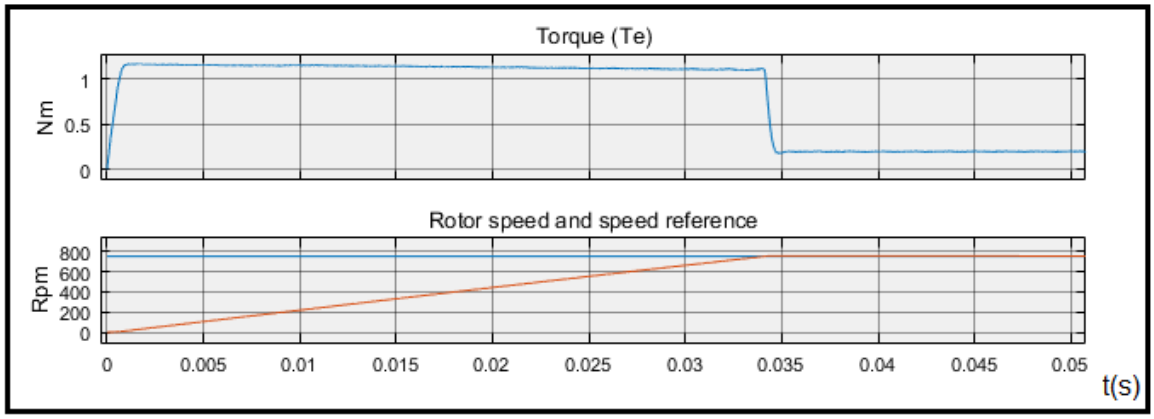

Figure 4.20: CMR system response - Mechanic start-up

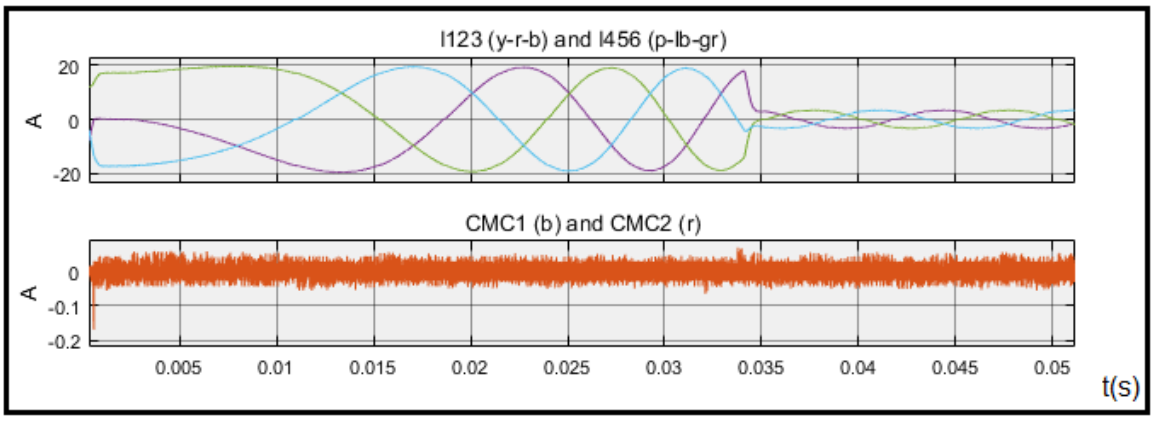

Figure 4.21: CMR system response - Electric start-up

4.3.2. CMR system behaviour - Steady state

The steady state period is simulated in a similar fashion as done previously for the original system, visualised in figure 4.22 and 4.23. The torque shows significant ripple effect and the rotor speed approaches the reference speed. the CMC waveform is no longer triangular and has a reduced magnitude compared to the original system. The stator currents also show the implementation of dead-time during the zero-crossing moments.

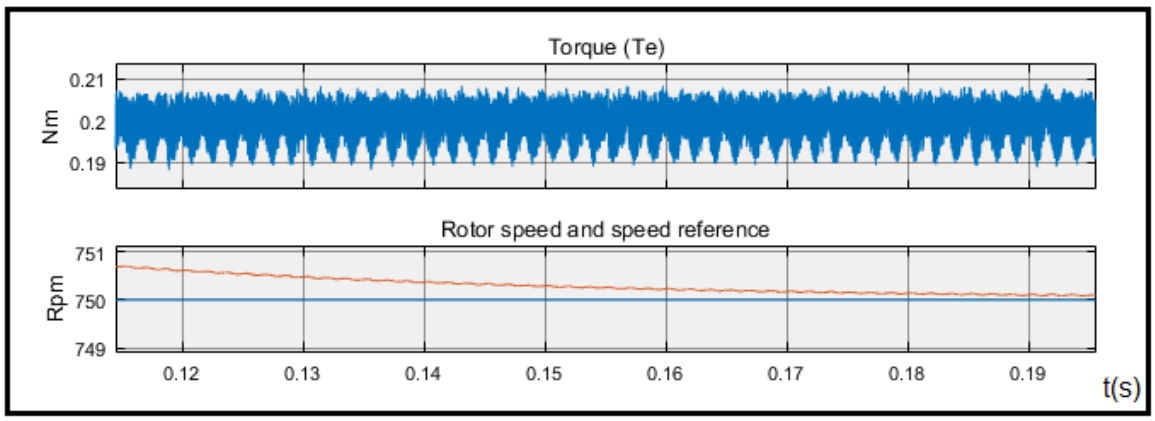

Figure 4.22: CMR system response - Mechanic steady state

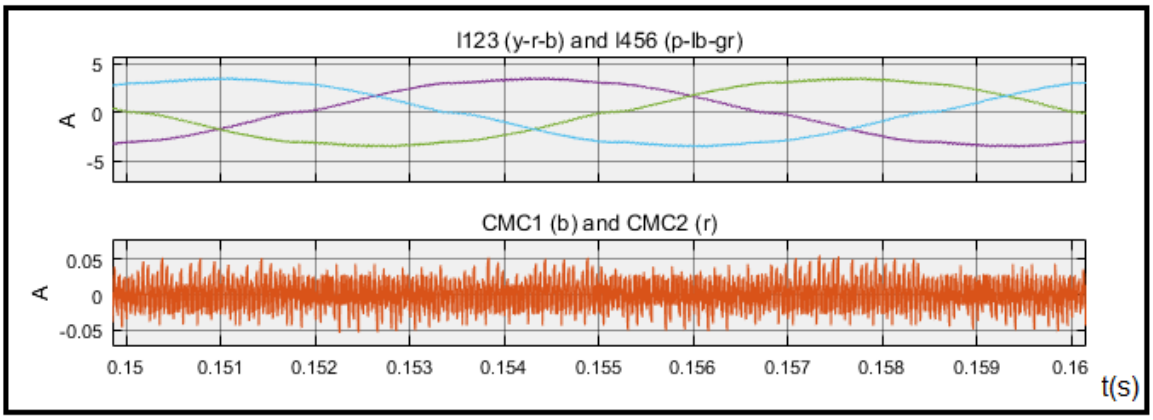

Figure 4.23: CMR system response - Electric steady state

4.3.3. CMR system behaviour - Post-OCF

The post-OCF performance is presented in figure 4.24 an 4.25. The main goal of this system is to maintain the operation of the remaining (five) phases in post-OCF condition, whilst also controlling the CMC. The post-OCF mechanic properties show oscillatory behaviour, this is considered acceptable, as the rotor speed is close to the reference. The current in the sound phase set increases and compensates for the faulted phase. The remaining phases in the faulted phase set are shifted 180°. CMC1 and CMC2 are not identical in post-OCF condition. The CMC is maintains pre-fault levels. This verifies the possibility to maintain operation when subjected to a fault.

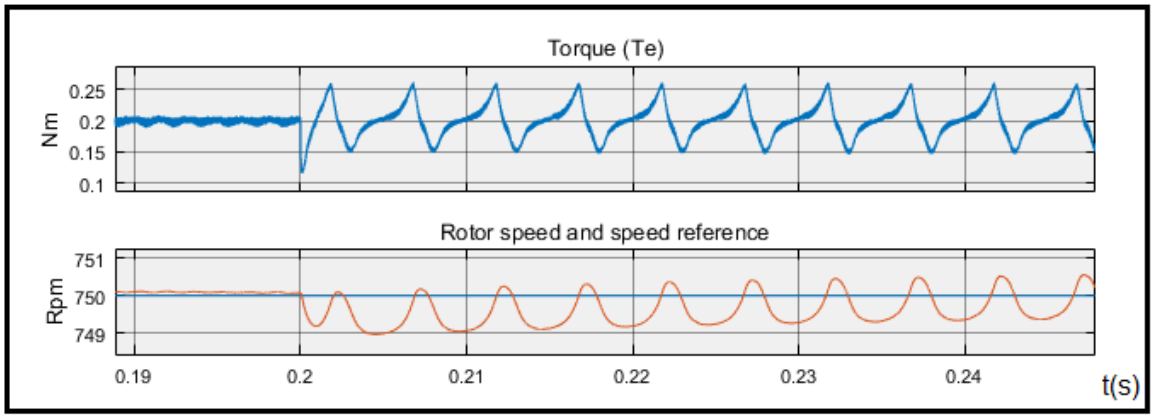

Figure 4.24: CMR system response - Mechanic post-OCF

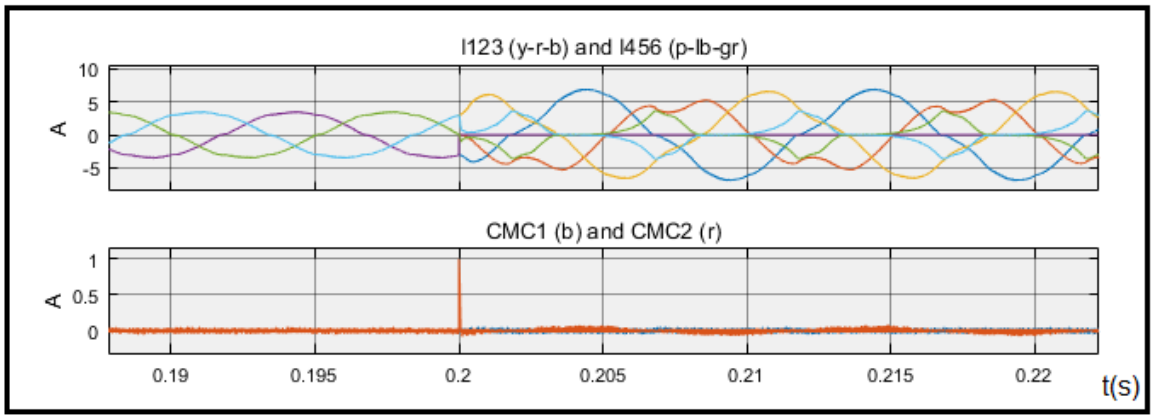

Figure 4.25: CMR system response - Electric post-OCF

Figure 4.26 and 4.27 visualise the final time period of the system response. The dynamic response due to a change in speed reference is visualised here. A step size increase of 10% shows an increase in torque, the rotor accelerating and settling at the new reference speed, a short increase in current and unaltered CMC.

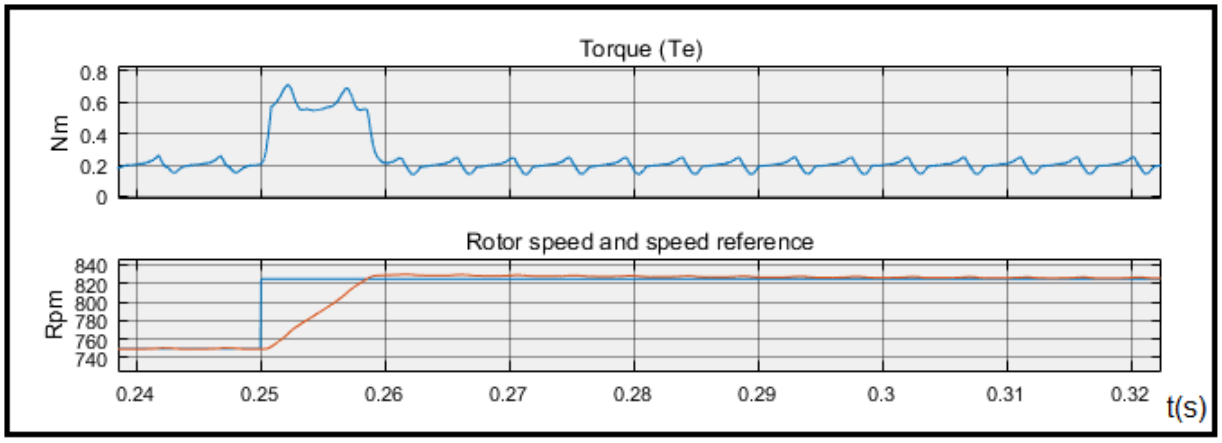

Figure 4.26: CMR system response - Mechanic post-OCF - Dynamic response

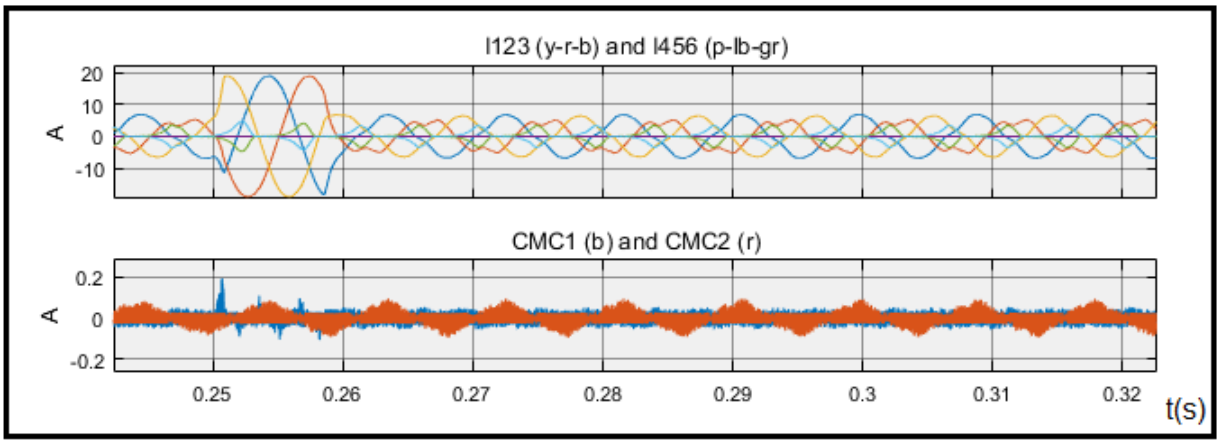

Figure 4.27: CMR system response - Electric post-OCF - Dynamic response

4.4. Comparison

A comparison is provided for the original system and the CMR control system with dead time implemented in table 4.4. This comparison shows that that the steady state current amplitude is also reduced in the CMR control system. The amplitude of the CMC in when applying CMR control was found to be smaller than in the original system. A drawback when applying the CMR control system is the increased settling time (ts).

Table 4.4: Comparison of converter performance - 750rpm - Vdc 45V - steady state

	Original system	**CMR system**
Is amplitude (A)	4.40	3.5
CMC1,2 (%)	12.07	1.43
ts 2% (ms)	33.01	33.40

Performance parameters for the post-OCF period are presented in table 4.5. The impact of the mechanic ripple is depends on the application, this should not be an issue for regular motor applications. For the post-OCF current amplitude it should be noted that the increase for the original system occurs in the faulted phase set, for the CMR system this occurs in the sound phase set. The increase in the sound phase set is more beneficial as the per phase power increase is spread over three phases instead of two.

Table 4.5: Comparison of converter performance - post-OCF - *sound phase set, **faulted phase set

	Original system	**CMR system**
Is amplitude (A)	**6.80	*6.92
CMC (%)	**56.62	*1.01
Te ripple (%)	38.00	28.00
n ripple (%)	0.17	0.18

4.4.1. Copper loss

The post-OCF power performance is compared by fixing the mechanical output power and calculate the necessary current to supply the load. The copper loss is a limiting factor for a machine and is largely dependant on the stator current. The copper loss is determined by the equation below for a pre-fault time period (t0 = 0.15s, te = 0.20s) and for the post-OCF time period (t0 = 0.12s, te = 0.25s), both in steady state condition.

$$P_{cu} = \frac{1}{t_e - t_0} \int_{t_0}^{t_e} i_s(t)^2 \cdot dt$$

Table 4.6 presents a copper loss comparison. The post-OCF copper loss is relative to the pre-fault loss. The maximum overload factor of an individual phase is 302.52% for the original and 344.21% for the CMR system. The total sum of the overloading factor is 880.07% for the original and 949.39% for the CMR system.

Table 4.6: Comparison of converter performance - Copper loss overloading factor - Phase 4 OCF

	Original system	**CMR system**
Pcu pre-fault - phase 1-6 (W)	0.6631 (100%)	0.6525 (100%)
Pcu post-OCF - phase 1	101.25%	45.23%
Pcu post-OCF - phase 2	101.54%	45.32%
Pcu post-OCF - phase 3	98.93%	344.21%
Pcu post-OCF - phase 5	275.83%	*221.30%
Pcu post-OCF - phase 6	302.52%	293.33%
Total post-OCF	880.07%	949.39%

4.5. Shortcomings

The simulation in this chapter covered the comparison of a low speed (750rpm) low voltage (45V) case. During this study several tests were performed at different speeds and voltages. These tests showed that the CMC in the original system decreased as a function of rotor speed. For the CMR system it showed that the determining factor of the magnitude of CMC was the voltage level of the DC bus. Performing tests on several test cases showed that the CMR system was not an improvement for a high speed (3000rpm) high voltage (540V) case. The results of multiple tests cases are presented in table 4.7 and 4.8.

Table 4.7: Common Mode current - Steady state - Original system

Vdc	**CMC @ 750rpm (A)**	**CMC @ 3000rpm (A)**
45V	0.5	0.26
270V	0.5	0.26
540V	0.5	0.26

Table 4.8: Common Mode current - Steady state - CMR system

Vdc	**CMC @ 750rpm (A)**	**CMC @ 3000rpm (A)**
45V	0.05	0.05
270V	0.25	0.25
540V	0.5	0.5

4.6. Discussion

The CMR system system has improved characteristics compared to the original system but is not superior in all aspects.

The CMC of the original system in post-OCF condition does not allow FT operation over an extended period of time. This is solved when applying the CMR control system. The new system allows the system to maintain operation at a nominal load, but subjected to a current overload of 344.21%. This is in contrast to the 50% post-OCF power reduction when disabling the faulted phase set, as would be the case in the original system due to the large CMC. The CMR control system provides an approach to facilitate FT control in the existing drive system whilst reducing the CMC during post-OCF condition.

The analysis of different tests cases (paragraph 4.5) revealed that the magnitude of the CMC was determined by the speed for the original control system, and the DC bus voltage for the CMR control system. It should be noted that the nominal parameters for the drive system are 540V for the DC bus and 60000rpm for the speed (paragraph 3.1). This means that the CMR control system is not an

improvement over the original control system for steady state (pre-fault) condition. It is questioned if the CMC is a problem for the original system at the rated speed.

It is possible to apply DC Bus Control (DBC) in case the converter is supplied by a controlled rectifier, this is beneficial to the CMR control as a lower DC bus voltage directly reduces the CMC. The maximum reduction of the DC bus voltage is determined by the loading of the machine. A FT machine has to be overdimensioned to allow post-OCF operation, this combinations might solve the shortcoming of the CMR control system.

5

Reliability assessment of converter topologies

As discussed in the chapter 2, it is stated that FT is not the same as reliability. However, it is stated that FT is related to impact and reliability to chance. The combination of impact and chance define risk. Literature on FT drive systems cover different types of converter topologies. A reliability assessment on FT converter topologies is considered as contribution to the current state of academics. Designing a system to be FT without considering reliability will prove unsatisfactory. This chapter will therefore introduce an approach to asses the reliability of the converter topologies that will result in a comparison of topologies. The approach of this chapter builds upon the findings of a by U. Shipurkar *et al.,* [32] as discussed in paragraph 2.7. This study presents failure rates for PMSM power converters as applied in wind turbines. These parameters can be used to compare topologies even when applied in aerospace engineering, as different converter topologies are subjected to similar per component failure rates. Additional literature was studied to provide a solid foundation on the failure rates. These studies were difficult to compare, as the categorisation of the failure rates was often not elaborated. The rates of this study are therefore based on one source [32]. It is recommended that additional research should be conducted, to determine the failure rates in power converters. Applying Markov chain models seem like a promising candidate to provide a comparison on FT converter topologies as there are several operating states to analyse.

5.1. Introduction to Markov chain

A Markov chain is a discrete stochastic model that describes the probability of a systems state in (discrete) time [35]. The application of this model on the converter topologies is done by defining the possible failure states and conditions per topology and combining those with failure rates [32]. This section will discuss the application of Markov chains on the topologies defined in paragraph 2.4, and how the failure rates and states are defined. The approach in this project is based on the book: Markov chains Models, Algorithms and Applications by W. Ching *et al.,* [35]. It is expected that the theory on Markov chains is not common knowledge in this field, therefore an example will be given regarding a weather case [36]. Figure 5.1 illustrates the the Markov chain model, in this figure two states are defined. The day is either sunny (S) or rainy (R). Fixed chances are applied for this example, the probability of a rainy day after a sunny day is set at 10% (λ1). The probability of a sunny day after a rainy day is set at 50% (λ2). Due to the nature of this example it can be claimed that the reverse probability applies. A sunny day therefore follows a sunny day at 100% - 10% = 90%. The probability of a rainy day following a rainy day is 50%. These probabilities are set in a probability Matrix P.

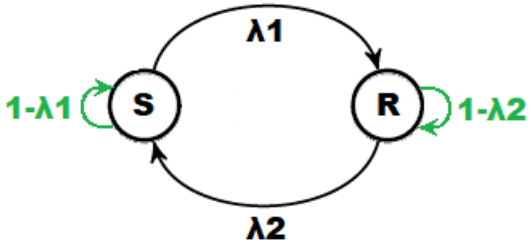

Figure 5.1: State-transition diagram - Case: Sunny-rainy example

$$P = \begin{bmatrix} 0.9 & 0.1 \\ 0.5 & 0.5 \end{bmatrix} = \begin{bmatrix} 1-\lambda 1 & \lambda 1 \\ \lambda 2 & 1-\lambda 2 \end{bmatrix}$$

The discrete time steps of this problem is set in days. Utilising the probability matrix in combination with the initial state formulated below, the states of the consecutive days can be calculated in the matrix vector equations below. X0 represents the initial state (day 1) which is 100% sunny. Multiplying that state with the probability matrix results in the probability of a sunny day on day 2 at 90%. Utilising substitution quickly results in the exponential equation where the probability distribution of any upcoming day can by determined by the exponential (n).

$$\underline{x_0} = \begin{bmatrix} 1 & 0 \end{bmatrix}$$
$$\underline{x_1} = \underline{x_0} P \begin{bmatrix} 0.9 & 0.1 \end{bmatrix}$$
$$\underline{x_2} = \underline{x_1} P = \underline{x_0} P^2 = \begin{bmatrix} 0.84 & 0.14 \end{bmatrix}$$
$$\underline{x_n} = \underline{x_0} P^n$$

5.2. Hourly Failure rates

The hourly failure rates of each converter component is presented in table 5.1. A total failure rate for PMSM systems is argued to be 1.32 converter failures per year [32]. The combination of this data and the failure distribution of figure 2.12 allow the determination of the hourly failure chance per component. By approaching these failure rates as probabilities it can also be stated that the inverse rate represents that the component is functioning. It is expected that there is no chopper in the application for aerospace engineering, this parameter is therefore excluded. A large portion of the failure rate was not specified (16%). It is considered necessary to remove this data from the study, as it is impossible to argue the impact of a fault of which the origin is unknown.

Table 5.1: Hourly failure rate per component - *Single IGBT (internal diode) module [32]

Component	Hourly failure rate (e-5)	Component	Hourly failure rate (e-5)
Rectifier	2.411	IGBT module*	0.371
Inverter	2.110	Passives	0.603
Control (Hw)	0.753	Control (Sw)	1.356
Fuses/Mech. switches	1.356	Conductor Board	1.356
Total	12.171		

5.3. Reliability assessment of converter topologies

The goal of the reliability assessment is to find quantitative data that can be used to compare FT converter topologies. Several topologies were presented in paragraph 2.4 and provide a starting point for this assessment. Three main categories in converter topologies were found: Traditional VSI, OW and the extra redundant switching leg. These converters can be realised in redundant layers, adding to

the overall reliability of the system. The final aspect covered in FT converter topologies is the inclusion of a common or split DC bus supply system.

- Topology.
- Number of phase sets.
- Common or Split DC bus.

By analysing these categories conclusions can be drawn on how to choose a FT converter topology. Presenting a comparison of these topologies and whether to apply a common or split DC bus. The amount of value added by applying layered redundant phase sets will also be analysed.

5.3.1. Assumptions

A comparison on FT converters can only be obtained if the converters are comparable. Several assumptions are formulated to do so:

- Only electric faults in the drive system are considered.
- Constant failure rates per component.
- The total failure rate can be determined by summing (the contributing) failure rates of the components.
- A repair interval of once every 24 hours, a repair will revert a FT state back to a Healthy state.
- Only single simultaneous faults are considered due to fault isolation (this fault does not impact the failure rates).
- An IGBT module fault will be treated as an OCF, this fault type will disable one phase or one phase set (depending on the topology).
- One inverter and control (Hw/Sw) module per set of three phases, this fault type will disable one set of phases.
- One rectifier, conductor board, passives and fuses/mech switch modules per DC bus, this fault type will disable the phases connected to that DC bus.

The limitation to electric fault resides in the definition of FT as formulated in chapter 2. It is common to incorporate fault isolation when designing a FT system. The assumption that only single simultaneous faults occur is therefore logical.

Constant failure rates are assumed for multiple reasons. The operating conditions of each converter type are not equal. A specific converter topology might be preferred depending on the application. Each converter topology is also subjected to different overrating factors, this likely results in an increased failure rate during FT operations modes. Neglecting this aspect simplifies the assessment.

Each state is associated with fixed operating component. Each operating component is associated with a constant failure rate. This leads to the assumption that the total failure rate of an operating mode can be determined by the sum of failure rates of the operating components.

Continued operation in a faulted condition is not favourable. Therefore it is assumed that a repair interval should be taken into account. A repair action will revert a FT state back to a H state. A 24 hour time period is considered a practical interval when considering aerospace applications, representing overnight repair.

The final three items cover the impact of a fault. Each of these assumptions is made primarily to simplify the analysis to an ideal case. Electric fault types can be an OCF, SCF or shutdown of the power supply. For an ideal/theoretical case that it always possible to revert a SCF to an open circuit, this can achieved by applying circuit breakers, fuses or additional semiconductor devices. Several examples are presented in a study by A. Welchko *et al.,* [12]. This assumption leads to a simple cause effect relation.

5.4. Traditional VSI

The traditional VSI is not a FT converter topology, but is often applied in redundant layers to achieve FT. The two layer application is presented in paragraph 2.4.1 which show two separate traditional VSI's.

5.4.1. VSI 1x3 phase

In order to compare topologies a reference case has to be formulated. Analysing the reliability of the traditional VSI in a three phase (1x3) configuration allow for a comparison in topologies without relying on redundancy. The state-transition diagram is therefore also simple, any fault will revert the system from a Healthy (H) to a Fauled (F) state.

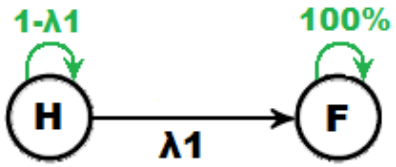

Figure 5.2: State-transition diagram - Case: Traditional VSI 1x3

Only two states are defined in this converter topology, Healthy (H) and Faulted (F). There are no possible FT states, the impact of repair time is therefore also nonexistent. The impact of a fault will cause the systems function to fault. The probability vector is determined in a similar way to the Markov chain example. This vector presents the probability distribution at the time interval displayed in the exponent. The probability of a faulted state was found at 71.80% over 10000 hours, the second (last) entry of the probability vector.

Table 5.2: State-transition parameter decomposition - Traditional VSI 1x3

Component	**#(λ1)**	**Component**	**#(λ1)**
Rectifier	1	IGBT modules	6
Inverter	1	Passives	1
Control (Hw)	1	Control (Sw)	1
Fuses/Mech. switches	1	Conductor Board	1

$$P = \begin{bmatrix} 1-\lambda 1 & \lambda 1 \\ 0 & 1 \end{bmatrix} \approx \begin{bmatrix} 0.9999 & 1.27e-4 \\ 0 & 1 \end{bmatrix}$$

$$\underline{x_0} = \begin{bmatrix} 1 & 0 \end{bmatrix}$$

$$\underline{x_{10000}} = \underline{x_0} P^{10000} \cdot 100\% = \begin{bmatrix} 28.2004\% & 71.7996\% \end{bmatrix}$$

5.4.2. Redundant traditional VSI 2x3 phase split DC

The first FT topology where Markov chains are applied is that of the redundant dual three phase topology (figure 5.3), as discussed in paragraph 2.4.1. The possible states of this topology are as followed: H, FT (1x3) and F. FT is the requirement of this study and is inherited in this system topology, as discussed in the literature study. The system falls in a FT state if any fault occurs in a single converter. No measures are taken to maintain operation with the faulted converter (set), the post-fault nominal output power will be 50%. The probability of a direct state transition between H and F is zero, this link does therefore not exist in the state-transition diagram. Setting the probability to remain in the faulted state at 100% allows the computation of the availability over 10000 operation hours, this failure state chance will accumulate as the exponent increases.

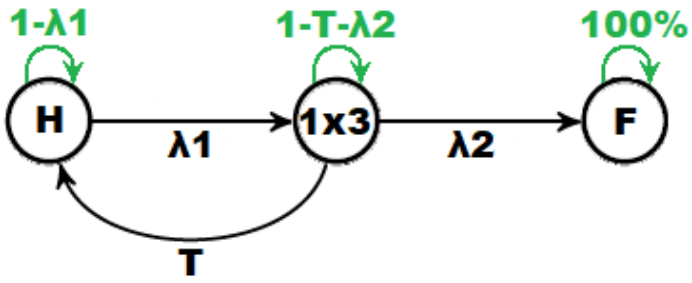

Figure 5.3: State-transition diagram - Case: Redundant dual three phase converter (2x3) split DC bus

The contributors to the failure rates per state is presented in table 5.3. This is done by allocating the contribution of a component to a state transition. The state-transition from H to FT (λ1) occurs if any component faults in either converter. Redundancy doubles the failure rate whilst reducing the impact of a fault. The system as a whole is expected to have two rectifier modules. For transition case between FT and F only six IGBT modules operate, these modules are therefore subjected to a non-zero fault chance. The expected comparison chance that the system is expected to fail over 10000 hours is found in the third entry of the probability vector, this chance is found at 0.76%.

Table 5.3: State-transition parameter decomposition - Redundant dual three phase converter (2x3) split DC bus

Component	**#(λ1)**	**#(λ2)**	**Component**	**#(λ1)**	**#(λ2)**
Rectifier	2	1	IGBT modules	12	6
Inverter	2	1	Passives	2	1
Control (Hw)	2	1	Control (Sw)	2	1
Fuses/Mech. switches	2	1	Conductor Board	2	1

$$P = \begin{bmatrix} 1-\lambda 1 & \lambda 1 & 0 \\ T & 1-T-\lambda 2 & \lambda 2 \\ 0 & 0 & 1 \end{bmatrix} \approx \begin{bmatrix} 0.9997 & 2.532e-4 & 0 \\ 0.0417 & 0.9582 & 1.266e-4 \\ 0 & 0 & 1 \end{bmatrix}$$

$$\underline{x_0} = \begin{bmatrix} 1 & 0 & 0 \end{bmatrix}$$

$$\underline{x_{10000}} = \underline{x_0} P^{10000} \cdot 100\% = \begin{bmatrix} 98.6451\% & 0.5975\% & 0.7574\% \end{bmatrix}$$

5.4.3. Redundant traditional VSI 2x3 phase common DC

The second FT case to be modelled as a Markov chain is that of the dual three phase converter with a common DC bus. This topology had a different take on the dual three phase topology and was previously discussed in paragraph 2.4.2. The different design results in a different probability matrix mainly because there is a non-zero failure rate of a transition between H to F, caused by the common DC bus. The sate-transition diagram of this topology is visualised in figure 5.4. the failure rate contributors to the transition parameters are presented in table 5.4.

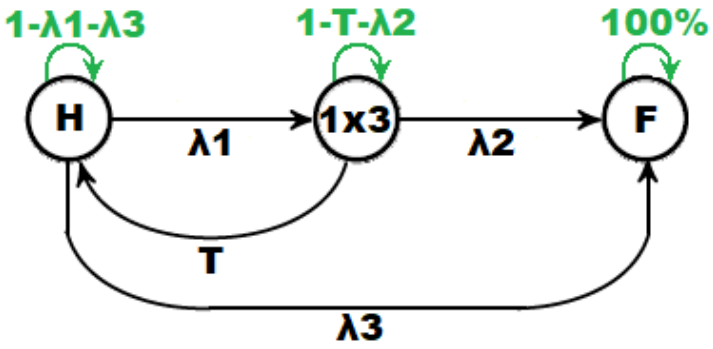

Figure 5.4: State-transition diagram - Case: Dual three phase converter (2x3) common DC bus

The composition of the initial failure rate (λ1) is done by analysing which component fault will cause the system to transition from a H state to the FT (1x3) state. A failure any of the 12 IGBT modules will cause this transition, a failure in any of the two inverters and control (Hardware (Hw) and Software (Sw)) modules will cause this transition. Any other failure will result in the other possible state transition (λ3).

Table 5.4: State-transition parameter decomposition - Dual three phase converter (2x3) common DC bus

Component	**#(λ1)**	**#(λ2)**	**#(λ3)**
Rectifier	0	1	1
IGBT modules	12	6	0
Inverter	2	1	0
Passives	0	1	1
Control (Hw)	2	1	0
Control (Sw)	2	1	0
Fuses/Mech. switches	0	1	1
Conductor Board	0	1	1

The probability matrix is determined by combining the previous data from paragraph 5.2 in combination with table 5.4. This matrix is constructed to represent the model visualised in figure 5.4. The probability distribution over 10000 hours is presented in bottom equation, the final entry represents the probability that the system has entered a F state over the time period, this probability is found at 43.72%.

$$P = \begin{bmatrix} 1-\lambda 1-\lambda 3 & \lambda 1 & \lambda 3 \\ T & 1-T-\lambda 2 & \lambda 2 \\ 0 & 0 & 1 \end{bmatrix} \approx \begin{bmatrix} 0.9998 & 0.0001 & 5.72e-5 \\ 0.0417 & 0.9582 & 0.0001 \\ 0 & 0 & 1 \end{bmatrix}$$

$$\underline{x_0} = \begin{bmatrix} 1 & 0 & 0 \end{bmatrix}$$

$$\underline{x_{10000}} = \underline{x_0} P^{10000} \cdot 100\% = \begin{bmatrix} 56.0983\% & 0.1864\% & 43.7153\% \end{bmatrix}$$

5.4.4. Redundant traditional VSI 3x3 phase

Expanding the traditional VSI topology to three layer redundancy is presented in this paragraph. The construction of this model is an expansion on the two layer model presented in paragraph 5.4.2. The converter is realised as three separate converters. A failure in any of the converters will operate with the remaining sets. The chance of a direct state transition between H and F is therefore nonexistent.

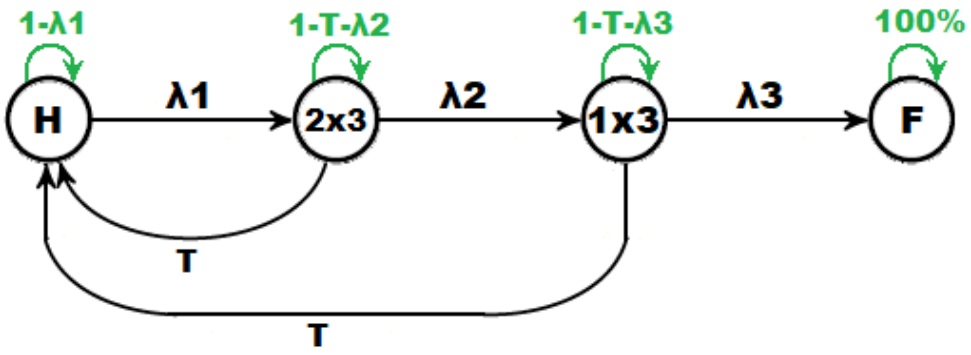

Figure 5.5: State-transition diagram - Case: Dual three phase converter with common DC bus

Table 5.5 presents the allocation to the state-transition parameters. Computing the expected failure probability is found at 6.8e-3%. Adding several decimals of reliability to the previous cases.

Table 5.5: State-transition parameter decomposition - Dual three phase converter (3x3)

Component	#(λ1)	#(λ2)	#(λ3)
Rectifier	3	2	1
IGBT modules	18	12	6
Inverter	3	2	1
Passives	3	2	1
Control (Hw)	3	2	1
Control (Sw)	3	2	1
Fuses/Mech. switches	3	2	1
Conductor Board	3	2	1

$$P = \begin{bmatrix} 1-\lambda 1 & \lambda 1 & 0 & 0 \\ T & 1-T-\lambda 2 & \lambda 2 & 0 \\ T & 0 & 1-T-\lambda 3 & \lambda 3 \\ 0 & 0 & 0 & 1 \end{bmatrix} \approx \begin{bmatrix} 0.9996 & 3.797e-4 & 0 & 0 \\ 0.0417 & 0.9581 & 2.532e-4 & 0 \\ 0.0417 & 0 & 0.9582 & 1.266e-4 \\ 0 & 0 & 0 & 1 \end{bmatrix}$$

$$\underline{x_0} = \begin{bmatrix} 1 & 0 & 0 & 0 \end{bmatrix}$$

$$\underline{x_{10000}} = \underline{x_0} P^{10000} \cdot 100\% = \begin{bmatrix} 99.0901\% & 0.8976\% & 0.0054\% & 0.0068\% \end{bmatrix}$$

5.5. OW

The OW converter is one of the FT converter topologies analysed in this reliability assessment. The working of this topology is presented in paragraph 2.4.4. The dual three phase OW with common DC bus is also the topology applied in the lab setup. An important aspect of the OW converter is the capability to continue operation with a faulted phase set in case of an IGBT fault. The increase in failure rate due to the inclusion of extra IGBT modules should ideally be compensated by this aspect. The OW converter is a converter that is capable of operating when subjected to a fault. For this assessment it is assumed that each phase set is able to operate under condition of a single OCF per phase set.

5.5.1. OW 1x3phase

The OW converter can be realised in a three phase (1x3) configuration. The state-transition diagram is similar to the traditional VSI (2x3 with common DC bus) subjected to different state-transition parameters and a different FT state. The OW converter is able to operate subjected to an IGBT fault (λ1). Any other fault will cause the system to stop functioning (λ3).

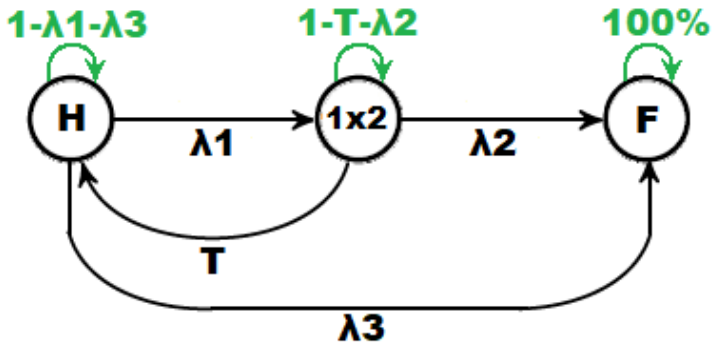

Figure 5.6: State-transition diagram - Case: OW (1x3)

Table 5.6: State-transition parameter decomposition - OW (1x3)

Component	#(λ1)	#(λ2)	#(λ3)
Rectifier	0	1	1
IGBT modules	12	8	0
Inverter	0	1	1
Passives	0	1	1
Control (Hw)	0	1	1
Control (Sw)	0	1	1
Fuses/Mech. switches	0	1	1
Conductor Board	0	1	1

The combination of the state-transition diagram (figure 5.6) and the parameter allocation of table 5.6 allow the construction of the probability matrix. Computing the probability of a failed state over 10000hours is found at roughly 63.03%.

$$P = \begin{bmatrix} 1-\lambda 1-\lambda 3 & \lambda 1 & \lambda 3 \\ T & 1-T-\lambda 2 & \lambda 2 \\ 0 & 0 & 1 \end{bmatrix} \approx \begin{bmatrix} 0.9998 & 5.42e-4 & 9.95e-5 \\ 0.0417 & 0.9582 & 1.36e-4 \\ 0 & 0 & 1 \end{bmatrix}$$

$$\underline{x_0} = \begin{bmatrix} 1 & 0 & 0 \end{bmatrix}$$

$$\underline{x_{10000}} = \underline{x_0} P^{10000} \cdot 100\% = \begin{bmatrix} 36.9229\% & 0.0480\% & 63.0291\% \end{bmatrix}$$

5.5.2. OW 2x3 phase with common DC bus

The analysis of the OW with common DC bus is performed in a similar way as the other topologies. The state transition diagram is very large for the OW converter for multiple phase sets, this due to the FT capabilities per phase set of the OW converter. The state-transition diagrams will therefore not be presented in this report as it offers no clarification.

Many states can be derived for a double OW converter, this is due to the stacking attribute of reduces phase operation. The defined states of this configuration are as followed: 2x3, 1x3 + 1x2, 2x2, 1x3, 1x2 and faulted. The defined states also reflect in the dimensions of the probability matrix, which is 6x6 for a state-transition diagram of six states. Column six of the probability matrix shows that there is a non-zero chance of an instant failure, this is because of the common DC bus. Any fault in the rectifier, fuses/Mech. switches or conduction board will terminate the power supply, effectively failing the system. The last entry of the probability vector shows the probability of a F state over the course of the time period at 43.64%.

$$P \approx \begin{bmatrix} 0.9997 & 1.08e-4 & 0 & 8.44e-5 & 0 & 5.72e-5 \\ 0.0417 & 0.9581 & 5.42e-5 & 4.22e-5 & 4.22e-5 & 5.73e-5 \\ 0.0417 & 0 & 0.9582 & 0 & 1.57e-4 & 5.73e-5 \\ 0.0417 & 0 & 0 & 0.9582 & 5.42e-5 & 9.95e-5 \\ 0.0417 & 0 & 0 & 0 & 0.9582 & 1.36e-4 \\ 0 & 0 & 0 & 0 & 0 & 1 \end{bmatrix}$$

$$\underline{x_0} = \begin{bmatrix} 1 & 0 & 0 & 0 & 0 & 0 \end{bmatrix}$$

$$\underline{x_{10000}} = \underline{x_0} P^{10000} \cdot 100\% = \begin{bmatrix} 56.0971\% & 0.1456\% & 0.0002\% & 0.1135\% & 0.0003\% & 43.6434\% \end{bmatrix}$$

5.5.3. OW 2x3phase split DC bus

The next probability matrix is determined as done previously for the OW split DC bus converter, due to the four possible states this matrix size is 6x6. The main difference between the common and split DC bus is that column six is zero for the first three states (H, 1x3 + 1x2, 2x2). The inclusion of a split feeding system mitigates the impact of that fault type. The probability distribution over 10000 hours shows that the probability of a faulted state occurring in this time period is 0.47%.

$$P \approx \begin{bmatrix} 0.9997 & 1.08e-4 & 0 & 1.99e-4 & 0 & 0 \\ 0.0417 & 0.9581 & 5.43e-5 & 9.95e-5 & 9.95e-5 & 0 \\ 0.0417 & 0 & 0.9581 & 0 & 2.71e-4 & 0 \\ 0.0417 & 0 & 0 & 0.9582 & 5.42e-5 & 9.95e-5 \\ 0.0417 & 0 & 0 & 0 & 0.9582 & 1.36e-4 \\ 0 & 0 & 0 & & 0 & 01 \end{bmatrix}$$

$$\underline{x_0} = \begin{bmatrix} 1 & 0 & 0 & 0 & 0 & 0 \end{bmatrix}$$

$$\underline{x_{10000}} = \underline{x_0} P^{10000} \cdot 100\% = \begin{bmatrix} 98.8026\% & 0.2557\% & 0.0003\% & 0.4705\% & 0.0012\% & 0.4696\% \end{bmatrix}$$

5.5.4. OW 3x3phase split DC

Expanding the OW topology to three layer redundancy greatly increases the state-transition diagram and probability matrix. There will be no graphical representation of this case due to this. The construction of this topology is similar to the OW 2x3 phase split DC topology discussed in paragraph 5.5.3.

$$P \approx \begin{bmatrix} 0.999 & 1.63e-4 & 0 & 0 & 2.98e-4 & 0 & 0 & 0 & 0 & 0 \\ 0.042 & 0.958 & 1.08e-4 & 0 & 1.36e-4 & 1.99e-4 & 0 & 0 & 0 & 0 \\ 0.042 & 0 & 0.958 & 5.42e-5 & 0 & 2.71e-4 & 9.95e-5 & 0 & 0 & 0 \\ 0.042 & 0 & 0 & 0.958 & 0 & 0 & 4.07e-4 & 0 & 0 & 0 \\ 0.042 & 0 & 0 & 0 & 0.958 & 1.08e-4 & 0 & 1.99e-4 & 0 & 0 \\ 0.042 & 0 & 0 & 0 & 0 & 0.958 & 5.42e-5 & 9.95e-5 & 9.95e-5 & 0 \\ 0.042 & 0 & 0 & 0 & 0 & 0 & 0.958 & 0 & 2.71e-4 & 0 \\ 0.042 & 0 & 0 & 0 & 0 & 0 & 0 & 0.958 & 5.42e-5 & 9.95e-5 \\ 0.042 & 0 & 0 & 0 & 0 & 0 & 0 & 0 & 0.958 & 1.36e-4 \\ 0 & 0 & 0 & 0 & 0 & 0 & 0 & 0 & 0 & 1 \end{bmatrix}$$

From this matrix is can be observed that nine states are defined. Several FT states are defined. Many of these states are due to the continued operation should a phase set fault. Subcategories of these states are the continued operation in a set of phases should this be subjected to an IGBT fault. The probability that the system is found in a faulted state over 10000 hours is found at 3.3e-3%

5.6. Extra switching leg

The last major FT converter topology type includes extra switching legs to facilitate FT. The theory of these topologies were discussed in paragraph 2.4.3. The major difference between the traditional VSI

and the extra switching leg VSI is that an IGBT OCF will not cause the set to enter a failed state, the extra switching leg is used instead. These added switching leg are operational in pre-fault condition as a connection to ground is provided, the extra leg will contribute to the failure rate in all states.

5.6.1. Extra switching leg - 1x3 phase

The three phase system is first analysed similar to the other topologies. The state-transition diagram of this model is the same as a previous case (figure 5.4), the state transition parameters are not. The contribution to these parameters are presented in table 5.7. The state transition from H to FT is only possible in case of a fault in any of the eight IGBT modules. Any other fault during the H state will cause the system to stop functioning. Any subsequent fault in FT state will cause the system to transition to a F state.

Table 5.7: State-transition parameter decomposition - Redundant FT switching leg (1x3)

Component	#(λ1)	#(λ2)	#(λ3)
Rectifier	0	1	1
IGBT modules	8	6	0
Inverter	0	1	1
Passives	0	1	1
Control (Hw)	0	1	1
Control (Sw)	0	1	1
Fuses/Mech. switches	0	1	1
Conductor Board	0	1	1

The combination of the rates in paragraph 4.2 with the state transition parameters of table 5.7 allows the determination of the probability matrix. Computing the probability distribution over the same time period as previously. Computing the probability vector presents the chance of a F state at 61.18%.

$$P = \begin{bmatrix} 1-\lambda 1-\lambda 3 & \lambda 1 & \lambda 3 \\ T & 1-T-\lambda 2 & \lambda 2 \\ 0 & 0 & 1 \end{bmatrix} \approx \begin{bmatrix} 0.9998 & 3.616e-5 & 9.644e-5 \\ 0.0417 & 0.9582 & 0.0001 \\ 0 & 0 & 1 \end{bmatrix}$$

$$\underline{x_0} = \begin{bmatrix} 1 & 0 & 0 \end{bmatrix}$$

$$\underline{x_{10000}} = \underline{x_0} P^{10000} \cdot 100\% = \begin{bmatrix} 38.7898\% & 0.0336\% & 61.1766\% \end{bmatrix}$$

5.6.2. Extra switching leg - 2x3 phase common DC

The expanded case of the redundant switching leg is also investigated in this chapter. The original study stated that the three phase application had several shortcomings [15]. An additional system state is found when analysing the failure modes of this topology, due to the redundancy of this topology. The state-transition diagram of figure 5.7 which visualises the construction of the Markov chain model.

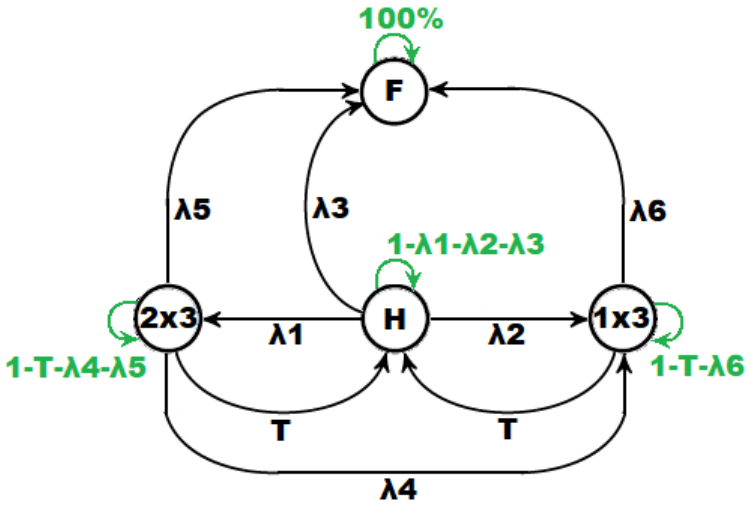

Figure 5.7: State-transition diagram - Case: Redundant FT switching leg (6phase)

The states of this model are: H, 2x3 for one of the FT states, 1x3 for the other FT state and F. Table 5.8 presents the state-transition parameter decomposition. The failure of any of the 14 IGBT modules during the H state will result in the transition from the H to the 2x3 FT state. The effect of utilising a common DC bus is that a failure probability exists (λ3) that results in an instant failure of the system.

Table 5.8: State-transition parameter decomposition - Redundant FT switching leg (six phase)

Component	#(λ1)	#(λ2)	#(λ3)	#(λ4)	#(λ5)	#(λ6)
Rectifier	0	0	1	0	1	1
IGBT modules	14	0	0	12	0	6
Inverter	0	2	0	1	0	1
Passives	0	0	1	0	1	1
Control (Hw)	0	2	0	1	0	1
Control (Sw)	0	2	0	1	0	1
Fuses/Mech. switches	0	0	1	0	1	1
Conductor Board	0	0	1	0	1	1

The probability matrix for this converter topology is defined by combining table 5.8 with data presented in paragraph 5.2. The probability matrix values are rounded, this is necessary due to the differences between the state transition parameters. The dimensions of the probability matrix is larger in this example due to the additional possible states of the system, four possible states result in a 4x4 probability matrix. The entries of the probability vector are from left to right: H, 2x3, 1x3 and F. The probability of a faulted state over the time period is found at 43.67%.

$$P = \begin{bmatrix} 1-\lambda1-\lambda2-\lambda3 & \lambda1 & \lambda2 & \lambda3 \\ t & 1-t-\lambda4-\lambda5 & \lambda4 & \lambda5 \\ t & 0 & 1-t-\lambda6 & \lambda6 \\ 0 & 0 & 0 & 1 \end{bmatrix} \approx \begin{bmatrix} 0.9998 & 6.329e-5 & 8.438e-5 & 5.726e-5 \\ 0.0417 & 0.9582 & 9.644e-5 & 5.726e-5 \\ 0.0417 & 0 & 0.9582 & 0.0001 \\ 0 & 0 & 0 & 1 \end{bmatrix}$$

$$\underline{x_0} = \begin{bmatrix} 1 & 0 & 0 \end{bmatrix}$$

$$\underline{x_{10000}} = \underline{x_0} P^{10000} \cdot 100\% = \begin{bmatrix} 56.1327\% & 0.0851\% & 0.1137\% & 43.6685\% \end{bmatrix}$$

5.6.3. Extra switching leg - 2x3 phase split DC

The extra switching leg converter topology can also be applied in double layer redundancy. A fault in the converters will allow a FT state that functions on one of two converters. This topology also allows an IGBT module fault in both converters as the added switching leg is then enabled. The state-transition diagram is chaotic due to the number of states. Therefore only the probability matrix is presented.

$$P \approx \begin{bmatrix} 0.9997 & 7.233e-5 & 0 & 1.989e-4 & 0 & 0 \\ 0.042 & 0.9581 & 3.616e-5 & 2.260e-4 & 0 & 0 \\ 0.042 & 0 & 0.9581 & 0 & 2.532e-4 & 0 \\ 0.042 & 0 & 0 & 0.9582 & 3.616e-5 & 9.9452e-5 \\ 0.042 & 0 & 0 & 0 & 0.9582 & 1.266e-4 \\ 0 & 0 & 0 & 0 & 0 & 1 \end{bmatrix}$$

The matrix portrays several important characteristics. Four FT states are defined and can be analysed by the parameters in row two, three, four and five. From the first row (H state) it can be seen that there is no direct link to the F state. Any conceivable fault analysed in this study will result in a 1x3phase operation (row 3) or a 2x3phase operation that utilises the extra switching leg (row 2). The probability of a failed state in 10000 hours is found at 0.47%.

5.6.4. Extra switching leg - 3x3 phase split DC

The final topology analysed in this study is the extra switching leg topology with three layer redundancy. Each set of phases is supplied by a separate DC bus and have an extra switching leg per phase set. The analysis of this topology assumed that the extra leg is subjected to a failure chance in H condition, as these provide a neutral connection. Only the last entry of the probability will be presented due to the size of the probability matrix (10x10) and the state-transition diagram. The probability that the system is found in a faulted state over 10000hours if found at 3.3e-3%

5.7. Comparison

Many topologies were covered in this chapter, each topology also presented a failure probability over a time period of 10000 hours. This section aims to provide an overview of the results that can be used to compare the topologies. Two conclusions are derived from this reliability assessments: The reliability of converter topologies and the possibility of redundant layering. Also the inclusion of a common versus a split DC bus supply system.

5.7.1. Reliability comparison of the converter topologies

The probabilities presented in the previous sections are summarised in table 5.9 for each topology. The percentage displayed are the probabilities of a failed state over the time period, a low value is therefore preferable. The table shows that the traditional VSI topology offers the highest failure probability in all phase set categories. The OW converter and the extra switching leg have a comparable reliability, and are slightly better than the traditional VSI. The reliability assessment in this study does assume that the failure rates are fixed for each topology.

Table 5.9: Faulted state probability over 10000 hours when repaired every 24hours (t) - Split DC bus converter topologies

	Traditional VSI (%)	**OW (%)**	**Extra switching leg (%)**
1x3 phases	71.80	63.03	63.02
2x3 phases	0.76	0.47	0.47
3x3 phases	6.8e-3	3.3e-3	3.3e-3

5.7.2. Common versus split DC bus

Similar to the previous section the comparison of applying a common versus split DC bus is presented in table 5.10. Each of these cases are for two sets of three phases. A major difference between the failure probability can be observed in each of the topologies. The main cause of this difference are the impact of faults in the rectifier, passive components, switchboard and fuses. These faults transition to a faulted state directly, the advantage of redundancy is lost for these fault types.

Table 5.10: Reliability comparison of applying a common versus split DC bus over the main converter topologies

	Traditional VSI (%)	OW (%)	Extra switching leg (%)
Split DC bus	0.76	0.47	0.47
Common DC bus	43.72	43.64	43.67

5.7.3. FT output power and cost factor

The reliability assessment as presented in the previous paragraph would be sufficient in case of similar hardware, this is not the case. It is therefore essential to analyse the FT power output and the cost that is associated to the reliability of the converter.

Table 5.11 presents the relative output power of the converter topologies when subjected to a (initial) fault [12]. The standard VSI (1x3) does not have a FT operation mode when subjected to a fault.

Table 5.11: Post fault nominal power output in the analysed topologies [12]

Converter	1x3	2x3	3x3
Standard	-	50%	67%
OW	58%	79%	86%
Extra switching leg	58%	79%	86%

The cost can be represented by the Silicon Overrating Cost Factor (SOCF) [12]. The standard VSI is utilised as a reference, the overrating factor represents the addition of semiconductor devices and the increased semiconductor power rating.

Table 5.12: Silicon overrating cost factor [12]

Converter	SOCF
Standard	1
OW	1.15
Extra switching leg	1.58

5.8. Discussion

Several aspects were analysed in this chapter. A comparison was drawn between converter topologies, layered redundancy, the effect of applying of a common DC bus, the cost and the overrating factor. It was found that the biggest gain is obtained when applying two layer (2x3) redundancy for each converter topology. The extra switching leg and OW topology has the lowest failure rate of the converters and a higher FT power output compared to the traditional VSI. The extras switching leg converter is subjected to the highest SORF of 1.58. The relative small gain in reliability with respect to the increased cost leads to the conclusion that the traditional VSI is a cost effective converter for FT drive systems, if applied redundant. The disadvantage of applying a traditional VSI is that over sizing or added redundant layers are expected to meet the FT power demand.

6

Conclusion

The main objective of this thesis is to determine how the existing drive system can be improved with regard to FT. Two topics were covered to reach this objective.

1. A case study was performed on the existing drive system that did not have a FT control system. A simulation model was constructed in Matlab Simulink that allowed the design of this FT control system. Several points of improvement were formulated for the existing setup. First was to solve the CM disturbance that occurred due to the SVPWM switching technique. Second was the implementation of a post-fault control strategy, utilising the remaining (five) sound phases in case of a fault. It was proposed that an expansion from dq to dq0 control might solve both points for improvement. Simulating the new control system confirmed this for the test case. Further analysis on both control systems showed that each have a different relation to the magnitude of the CMC. For the original system it is found that the CMC decreases as the rotor speed increases. The CMR system found that the CMC increases as the DC bus voltage increases. This in combination with the (very) high nominal speed of the machine leads to the conclusion that the original control system leads to a higher performance in (pre-fault) steady state condition for the existing setup. However, the CMC in post-fault condition and during start-up is very high for the original system. This leads to the conclusion that these control systems do not offer a high performance individually.

2. The reliability assessment was performed by applying Markov chain models. It was found that there were several different approaches to FT converter designs in literature. Three converter categories were formulated from literature: Traditional (redundant) VSI, OW and extra switching leg. Each topology was asses for zero, two and three layer redundancy. This assessment found that applying two layer redundancy offers the highest reduction in failure rate. Applying a common DC bus significantly reduces the reliability of the system, applying a split DC bus is considered more favourable for FT systems. The extra switching leg and OW converter topology both have a lower failure rate compared to the traditional VSI, but are also subjected to a higher overrating factor. The relative small gain in availability with respect to the increased cost leads to the conclusion that the traditional VSI is a cost effective converter for FT drive systems, if applied redundant.

The overall conclusion of this thesis is that the CMR control system offers a solution to incorporate FT in the existing drive system. This is mainly due to the requirement to reduce the CMC.

6.1. Recommendations

Several recommendations are formulated by the author for continued research.

- Reconsider the choice of FT converter topology in the existing setup.
- Expanding the reliability assessment with more data on reliability, especially for the power rating of the modules.
- Expand the reliability assessment by further analysing multiple fault types, expanded failure rates and the influence of FT operation modes on the failure rate.
- Practical implementation of CMR control in the existing setup to verify the simulation model.
- Further investigate the effect of the CMC waveform on the potential damage in the bearings.
- Investigate incorporating DBC in combination with the CMR control system to reduce the CMC for pre-fault steady state condition.
- Determining the rotor position in post-fault condition without encoder.
- Consider if the application a pre-fault (original) and a post-fault (CMR) control system in parallel.

Bibliography

[1] C. Kumar, "Sensorless Field Oriented Control in Modular Design Six Phase Permanent Magnet Synchronous Machine," MSc. thesis, TU Delft, 2016.

[2] W. Cao, B. C. Mecrow, G. J. Atkinson, J. W. Bennett and D. J. Atkinson, "Overview of Electric Motor Technologies Used for More Electric Aircraft (MEA)," in *IEEE Transactions on Industrial Electronics,* vol. 59, no. 9, pp. 3523-3531, Sept. 2012.

[3] B. C. Mecrow, A. G. Jack, J. A. Haylock and J. Coles, "Fault tolerant permanent magnet machine drives," *1995 Seventh International Conference on Electrical Machines and Drives (Conf. Publ. No. 412),* Durham, UK, 1995, pp. 433-437.

[4] D. J. Atkinson, S. Green, B. G. Mecrow, A. G. Jack and J. R. Coles, "Fault tolerant fuel pump drives for the all electric aircraft," *IEE Colloquium on All Electric Aircraft (Digest No. 1998/260),* London, UK, 1998, pp. 1/1-1/6.

[5] J. J. Wolmarans, M. B. Gerber, H. Polinder, S. W. H. de Haan, J. A. Ferreira and D. Clarenbach, "A 50kW integrated fault tolerant permanent magnet machine and motor drive," *2008 IEEE Power Electronics Specialists Conference,* Rhodes, 2008, pp. 345-351.

[6] J. Xu, Y. Yuan, Z. Zhang and H. Guo, "The influence analysis of different fault modes on the post-fault performance of fault tolerant permanent magnet synchronous motor," *2017 20th International Conference on Electrical Machines and Systems (ICEMS),* Sydney, NSW, 2017, pp. 1-5.

[7] E. Hill and S. J. Mountain, "Control of a variable speed, fault-tolerant permanent magnet generator," *2002 International Conference on Power Electronics, Machines and Drives (Conf. Publ. No. 487),* Sante Fe, NM, USA, 2002, pp. 492-497.

[8] A. G. Jack, B. C. Mecrow and J. Haylock, "A comparative study of permanent magnet and switched reluctance motors for high performance fault tolerant applications," *IAS '95. Conference Record of the 1995 IEEE Industry Applications Conference Thirtieth IAS Annual Meeting,* Orlando, FL, USA, 1995, pp. 734-740 vol.1.

[9] E. Levi, "Multiphase Electric Machines for Variable-Speed Applications," in *IEEE Transactions on Industrial Electronics,* vol. 55, no. 5, pp. 1893-1909, May 2008.

[10] T. Jonsky, H. Borcherding, P. Szymanski, J. Wettlaufer and M. Theßeling, "Comparison of control methods for H-bridge fed five-phase permanent magnet synchronous motors," *2016 18th European Conference on Power Electronics and Applications (EPE'16 ECCE Europe),* Karlsruhe, 2016, pp. 1-10.

[11] N. Bianchi, M. D. Pre, G. Grezzani and S. Bolognani, "Design considerations on fractional-slot fault-tolerant synchronous motors," *IEEE International Conference on Electric Machines and Drives, 2005.,* San Antonio, TX, 2005, pp. 902-909.

[12] B. A. Welchko, T. A. Lipo, T. M. Jahns and S. E. Schulz, "Fault tolerant three-phase AC motor drive topologies; a comparison of features, cost, and limitations," *IEEE International Electric Machines and Drives Conference, 2003. IEMDC'03.,* Madison, WI, USA, 2003, pp. 539-546 vol.1.

[13] N. Mohan, T.M.Underland, W.P.Robbins, *Power electronics converters, application and design.* NewYork: John Wiley and Sons, 2nd ed.

[14] W. Wang, J. Zhang, M. Cheng and S. Li, "Fault-Tolerant Control of Dual Three-Phase Permanent-Magnet Synchronous Machine Drives Under Open-Phase Faults," in *IEEE Transactions on Power Electronics,* vol. 32, no. 3, pp. 2052-2063, March 2017.

[15] O. Wallmark, L. Harnefors and O. Carlson, "Control Algorithms for a Fault-Tolerant PMSM Drive," in *IEEE Transactions on Industrial Electronics,* vol. 54, no. 4, pp. 1973-1980, Aug. 2007.

[16] H. Zhan, Z. Zhu and M. Odavic, "Analysis and Suppression of Zero Sequence Circulating Current in Open Winding PMSM Drives With Common DC Bus," in *IEEE Transactions on Industry Applications,* vol. 53, no. 4, pp. 3609-3620, July-Aug. 2017.

[17] Y. Zhou and H. Nian, "Zero-Sequence Current Suppression Strategy of Open-Winding PMSG System With Common DC Bus Based on Zero Vector Redistribution," in *IEEE Transactions on Industrial Electronics,* vol. 62, no. 6, pp. 3399-3408, June 2015.

[18] X. Zhang and K. Wang, "Current Prediction Based Zero Sequence Current Suppression Strategy for the Semicontrolled Open-Winding PMSM Generation System With a Common DC Bus," in *IEEE Transactions on Industrial Electronics,* vol. 65, no. 8, pp. 6066-6076, Aug. 2018.

[19] Ronghua Cui, Ying Fan, X. Zhang, Weixia Zhu and Ming Cheng, "A new fault-tolerant control strategy for switch open-circuit fault in open-winding driving system," *IECON 2016 - 42nd Annual Conference of the IEEE Industrial Electronics Society,* Florence, 2016, pp. 2141-2146.

[20] M. Senol, M. Schubert, G. Engelmann, R. W. De Doncker, T. Grosse and K. Hameyer, "Field oriented modeling and control of six phase, open-delta winding, interior permanent magnet synchronous machines considering current unbalance and zero sequence currents," *2016 IEEE Applied Power Electronics Conference and Exposition (APEC),* Long Beach, CA, 2016, pp. 643-650.

[21] Z. Zhou, C. Xia, Y. Yan, Z. Wang and T. Shi, "Disturbances Attenuation of Permanent Magnet Synchronous Motor Drives Using Cascaded Predictive-Integral-Resonant Controllers," in *IEEE Transactions on Power Electronics,* vol. 33, no. 2, pp. 1514-1527, Feb. 2018.

[22] J. J. Wolmarans, H. Polinder, J. A. Ferreria and D. Clarenbach, "Modular sensorless control of high speed, fault tolerant machines," *The 2010 International Power Electronics Conference - ECCE ASIA -,* Sapporo, 2010, pp. 2533-2539.

[23] M. Lambeck and M. Schrodl, "PSM drives with fault-tolerant position detection," Twentieth Annual IEEE Applied Power Electronics Conference and Exposition, 2005. APEC 2005., Austin, TX, 2005, pp. 753-756 Vol. 2.

[24] R. Leidhold, "Position Sensorless Control of PM Synchronous Motors Based on Zero-Sequence Carrier Injection," in *IEEE Transactions on Industrial Electronics,* vol. 58, no. 12, pp. 5371-5379, Dec. 2011.

[25] M. E. Haque, Limin Zhong and M. F. Rahman, "A sensorless initial rotor position estimation scheme for a direct torque controlled interior permanent magnet synchronous motor drive," in *IEEE Transactions on Power Electronics,* vol. 18, no. 6, pp. 1376-1383, Nov. 2003.

[26] P. P. Acarnley and J. F. Watson, "Review of position-sensorless operation of brushless permanent-magnet machines," in *IEEE Transactions on Industrial Electronics,* vol. 53, no. 2, pp. 352-362, April 2006.

[27] P. Xu and Z. Q. Zhu, "Initial Rotor Position Estimation Using Zero-Sequence Carrier Voltage for Permanent-Magnet Synchronous Machines," in *IEEE Transactions on Industrial Electronics,* vol. 64, no. 1, pp. 149-158, Jan. 2017.

[28] R. De Doncker, D. W. J. Pulle, A. Veltman, *Advanced Electrical Drives. Analysis, Modelling and Control.* Springer, 2011

[29] J. W. Bennett, B. C. Mecrow, D. J. Atkinson and G. J. Atkinson, "Safety-critical design of electromechanical actuation systems in commercial aircraft," in *IET Electric Power Applications,* vol. 5, no. 1, pp. 37-47, January 2011.

[30] J. O. Estima and A. J. M. Cardoso, "A fault-tolerant permanent magnet synchronous motor drive with integrated voltage source inverter open-circuit faults diagnosis," *Proceedings of the 2011 14th European Conference on Power Electronics and Applications,* Birmingham, 2011, pp. 1-10.

[31] M. Cheng, J. Hang and J. Zhang, ”Overview of fault diagnosis theory and method for permanent magnet machine,” in *Chinese Journal of Electrical Engineering,* vol. 1, no. 1, pp. 21-36, Dec. 2015.

[32] U. Shipurkar, J. Dong, H. Polinder and B. Ferreira, ”Availability of Wind Turbine Converters with Extreme Modularity,” in *IEEE Transactions on Sustainable Energy.*

[33] H. Zhan, Z. Q. Zhu, M. Odavic and Y. Li, ”A Novel Zero-Sequence Model-Based Sensorless Method for Open-Winding PMSM With Common DC Bus,” in *IEEE Transactions on Industrial Electronics,* vol. 63, no. 11, pp. 6777-6789, Nov. 2016.

[34] en.wikipedia.org. (2018). Space Vector Modulation. [online] Available at: https://en.wikipedia.org/wiki/Space_vector_modulation [Accessed 3 Jul. 2018].

[35] W. Ching, M.K. Ng, *Markov Chains: Models, Algorithms and Applications*, New York, Springer, 2006.

[36] en.wikipedia.org. (2018). Examples of Markov chains. [online] Available at: https://en.wikipedia.org/wiki/Examples_of_Markov_chains [Accessed 2 Jul. 2018].